An experimental and computational comparison of the dynamic response variability in a turbine blade with under-platform dampers

An Experimental and Computational Comparison of the Dynamic Response Variability in a Turbine Blade with Under-Platform Dampers

Erhan Ferhatoglu†[1], Chiara Gastaldi†, Daniele Botto†, Stefano Zucca†

† Department of Mechanical and Aerospace Engineering, Politecnico di Torino, Corso Duca degli Abruzzi 24, 10129 Torino, Italy

ABSTRACT

In this paper, the nonlinear response variability in turbine bladed disks coupled with under-platform dampers (UPDs) is both numerically and experimentally investigated in detail. Non-uniqueness uncertainty of contact forces, which leads to different static force equilibria under the same nominal conditions, is shown as the main source of multiple responses. In the experiments, a previously designed test rig consisting of one blade and two UPDs is used to reveal the inherent kinematics of the friction force uncertainty. A large variability range is achieved in different tests while keeping all user-controlled inputs identical. On the computational side, the boundaries of the variability range are predicted by utilizing a recently developed numerical method. The loss factor of the system is exploited as an objective function to be minimized through an optimization algorithm. To compare the results, several cases with different excitation levels and pre-loads are studied. It is shown in most of the cases that the method is well-suited for the computation of nonlinear response boundaries. Experimentally measured variability range of the dynamic responses and contact forces is computationally obtained with a satisfactory level of accuracy. A slight deviation is also reported in few cases, particularly for highly nonlinear ones where the numerical model is not fully capable of replicating the non-ideal conditions achieved during the tests.

Keywords: Non-unique contact forces, Under-platform dampers, Turbine bladed disks, Nonlinear vibration, Uncertainty quantification, Variability range

[1] Corresponding Author
E-mail addresses: erhan.ferhatoglu@polito.it (Erhan Ferhatoglu), chiara.gastaldi@polito.it (Chiara Gastaldi), daniele.botto@polito.it (Daniele Botto), stefano.zucca@polito.it (Stefano Zucca)

1. INTRODUCTION

A great challenge in turbomachinery applications is to be able to decrease high stresses causing fatigue failure during operation [1]. Mitigation of large vibration amplitudes by utilizing friction damping technologies can now be considered as one of the most suitable ways, after an intensive investigation lasting more than 40 years in this research area. A widely used approach is to use friction dampers, which provide both energy dissipation and sealing function. A large number of studies have been successfully performed with different damper geometries, where several examples can be found in the literature [2-7].

Along with their dissipative capabilities, the nonlinear nature of friction dampers brings various peculiarities to interpret. One of them is the system's dynamic response variability obtained under nominally identical conditions. In the literature, various multiple responses have been reported during tests of the same system in different installations [8] or frequency sweeps [9]. It has been shown in [10] that several uncertainties associated to different phenomena may give rise to vibration response variability. A special type of these uncertainties arises due to the non-uniqueness of friction forces. This phenomenon has been studied in the contact mechanics community even more than three decades ago [11-13], while Yang and Menq introduced it to the turbomachinery community firstly in [14] on wedge dampers. In particular, according to the Coulomb's law, the absolute value of the tangential force for a fully stuck contact point should be less than its limit value, which is computed by the multiplication of the friction coefficient and the normal force at the same point. This provides a range of different possible values for the static component of the tangential force, which, in turn, becomes non-unique. As a result, dynamic response variability may occur if partial slip is achieved in the contacts.

Non-uniqueness of the tangential forces, which is referred to as *uncertainty* in this paper, has been reported in both experimental [15, 16] and computational [17, 18] studies of turbomachinery applications. It may provide a difference of 50 Hz in the resonance frequency between two consecutive tests [19]. Moreover, it has been shown in [20] that response amplitudes may vary up to ten times for the same excitation level with different initial guess values of static tangential forces. From the engineering point of view, the highest attention is generally focused on the response limits. In the literature, a few methods have been developed to estimate the boundaries in the context of non-unique friction forces. The authors of [14] utilized geometric relations in the kinematics of wedge dampers, while limit tangential forces were used in [21]. However, these two methods may not be capable of capturing the

boundaries for complex systems, since they are suitable only for macro slip friction motion. To overcome this limitation, a more systematic approach that uses an optimization algorithm has been developed very recently in [22]. The system's loss factor is used as the objective function to be minimized, and this enables the computation of the upper and the lower boundaries regardless of the system complexity. It should be noted that the number of studies for the computation of the variability range due to uncertainty phenomenon is quite limited in the literature; therefore, this research area is open and requires further investigation.

This paper presents a comparison of an experimental and computational investigation on the dynamic response variability of turbine bladed disks with under-platform dampers (UPDs). On the experimental side, multiple vibration responses that have already been measured in [16] are used. To demonstrate the fact that the response variability is resulted by the non-unique friction forces, the non-repeatability of the static contact forces is shown from different tests performed under the same nominal conditions. For the computational simulations, the same rig used in the tests is modeled with a commercial finite element software from which the system matrices can be extracted in a reduced order form and then used within a developed in-house code. The friction between the blade and UPDs is imposed by using contact elements in the reduced order model, and the numerical results are computed with a nonlinear solver built in the in-house code. The main goal here is to assess whether the range of multiple responses measured in the experiments [16] can be predicted by the boundaries numerically computed with the method developed in [22]. For this purpose, several case studies with different excitation levels and static pre-loads are presented. In addition to the nonlinear frequency response curves, contact forces with corresponding hysteresis cycles are also investigated. It is shown that most of the multiple responses as well as the variability range can be numerically estimated by using the approach developed in [22]. Although the method works quite well in most of the situations, a slight variation between experimental and computational results is also observed in few cases, particularly for highly nonlinear regimes.

It should be underlined that the main goal of this study is neither to propose a new numerical approach nor to perform new tests purposely performed for the variability phenomenon. Instead, this study is the first attempt to compare the range of experimental results with a systematic computational approach in the context of response variability that resulted from the non-uniqueness of friction forces. Although the numerical method utilized in this study has been computationally proven in [22], it is here challenged for the first time with the

experimental data set collected in [16]. The authors think that such a comparison brings a novel contribution to the literature, since the non-uniqueness of friction forces has been often ignored in the design of turbomachinery, and researchers can become more aware about its impacts on the system dynamics.

The paper is organized as follows. The test rig is described in Section 2. The computational background is briefly recapped in Section 3. The results for different cases are presented and thoroughly discussed in Section 4. The paper is concluded in Section 5.

2. TEST RIG FOR A TURBINE BLADE WITH UNDER-PLATFORM DAMPERS

The validation of mathematical models for the uncertainty phenomenon requires a specially designed experimental setup to be able to measure variable dynamic response amplitudes under the same nominal conditions. For this purpose, the results of a dedicated test rig, first developed in [15], is utilized in this study. Test setup had been designed such that the following main criteria are ensured during the test.

- The shape of the UPD should ensure a cross coupling between the tangential force of one contact side and the normal force of the opposite side. This is an essential property to obtain response variability for the same nominal conditions with successive tests.

- In addition to frequency responses, the test rig should have the capability of measuring contact forces and relative displacements between contact surfaces. This feature enables the interpretation of the inherent contact dynamics in operation and provides the link between the recorded dynamic response and the specific set of contact forces that produced it.

- The blade root should be clamped properly to minimize an additional damping contribution. The only friction effect should be supplied by the contact between the blade and UPDs.

Conventional test structures in laboratory conditions generally consist of one UPD pressed between two blades, where some examples can be found in [2, 23, 24]. This architecture is quite popular due to its simplicity and it can be used to effectively investigate in-phase and out-of-phase blade motion, however it does not allow for contact forces to be measured. Instead, one blade with two UPDs supported by auxiliary equipment is more convenient to this purpose. It enables the damper to be in contact with the blade on one side, while the other side can be used to measure friction forces. This is the strategy utilized also in the present

study and implemented in the test rig introduced in [15] where the reader may find all relevant details on its design and measuring procedures. A brief description of the relevant features of the test rig is given here for the sake of completeness.

Fig. 1a shows the main assembly of the test rig. The blade is fixed from the root by applying a clamping force (F_{CLAMP}) with a purposely designed mechanism in the main block. Two UPDs at each side are loaded with dead weights that simulate the static centrifugal force (CF) in real applications. It should be noted that UPDs are positioned between the blade and an L-shaped force separator. In this way, the contact force on the non-blade damper side is decoupled along two perpendicular directions through the force separator, which is kept in place by a fixed side block. This provides reaction forces (R) to be measured with load cells (LC) positioned in between the force separator and the fixed side block. The actual contact forces are then calculated by utilizing geometric relations [15]. Fig. 1b shows a closer top-view of the blade's under-platform. Two contact pads numbered with 1 and 2 are directly bolted to the blade and to the force separator, respectively. These pads are designed for practical reasons. They can be replaced easily to investigate different damper geometries without modifying the main setup. In this study, the geometry of the utilized damper (D) is flat on the blade side, while it is cylindrical on the force separator side. This ensures flat-on-flat and cylinder-on-flat contact surfaces on different damper sides, which enables the investigation of different kinematics. The blade is also excited with an electromagnetic shaker (F_{EXC}) from a slot close to the root. Fig. 1c also representatively shows the static force balance on the left damper. Here, as mentioned above, the contact forces at the cylindrical side (T_{cyl} and N_{cyl}) were previously calculated with the load cell values, by utilizing a geometric relation between the contact pad 2 and the force separator. The contact forces at the flat side (T_{flat} and N_{flat}) are then derived through the force equilibrium by assuming the inertia of the damper is negligible. Interested readers may refer to [15] for a more detailed explanations about the entire test rig.

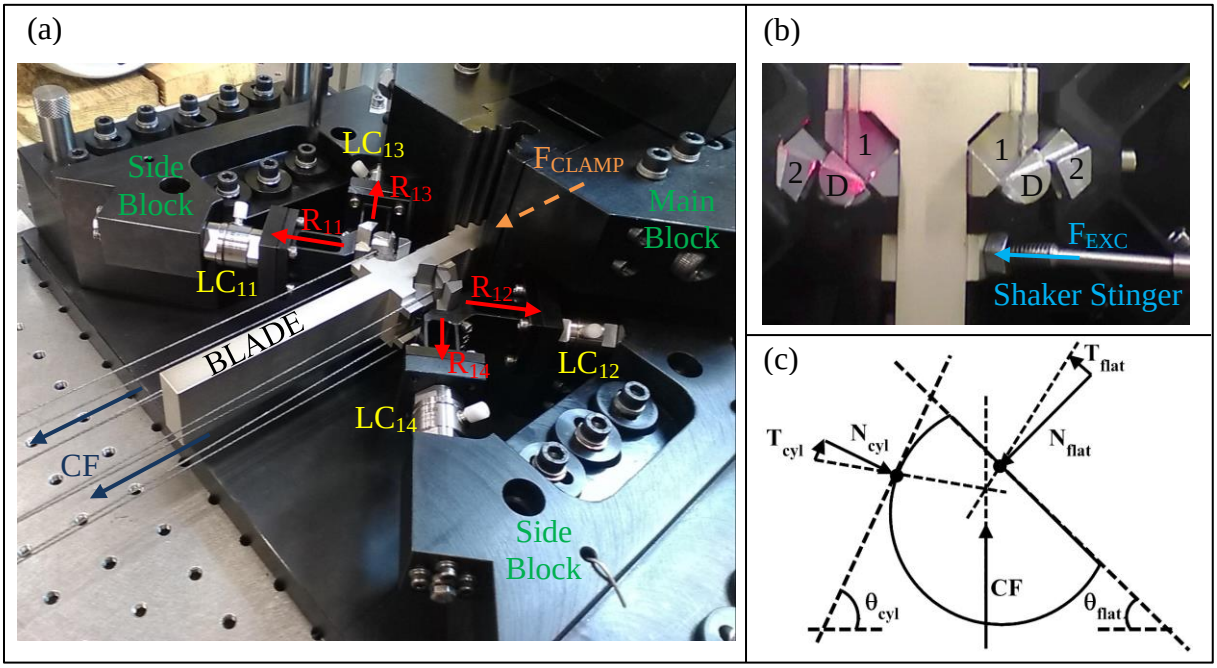

Fig. 1 (a) Test rig Setup, (b) A Closer view of the Blade's Under-platform, (c) Force Equilibrium on the Damper

The blade has been designed only for academic purposes and it imitates real turbine blades in the industry in terms of frequency range for the first modes. The first natural frequency corresponding to the lateral bending mode is designated to lie in the 400-450 Hz range. The blade is free from modal coupling and has a well-separated first lateral bending mode. An investigation on the clamping force has also been performed before starting the experimental campaign. No influence of root attachment has been observed for the clamping force values greater than 40 kN. Hence, F_{CLAMP} is set to 50 kN for all experiments. A standard force controlled stepped-sine testing has been utilized in the experiments to measure nonlinear frequency response functions (FRFs). Several sine sweeps have been performed with different excitation and centrifugal forces. The response of the blade tip is monitored with an accelerometer. Despite the fact that nonlinear FRFs are sufficient to observe the dissipation due to friction, the uncertainty phenomenon can only be interpreted in detail with the contact forces and hysteresis cycles. In order to measure these quantities, LCs are used to record contact forces as explained above, while a differential laser measures the relative displacement between the damper and contact pads. Fig. 2 briefly summarizes the complete experimental setup and flowchart.

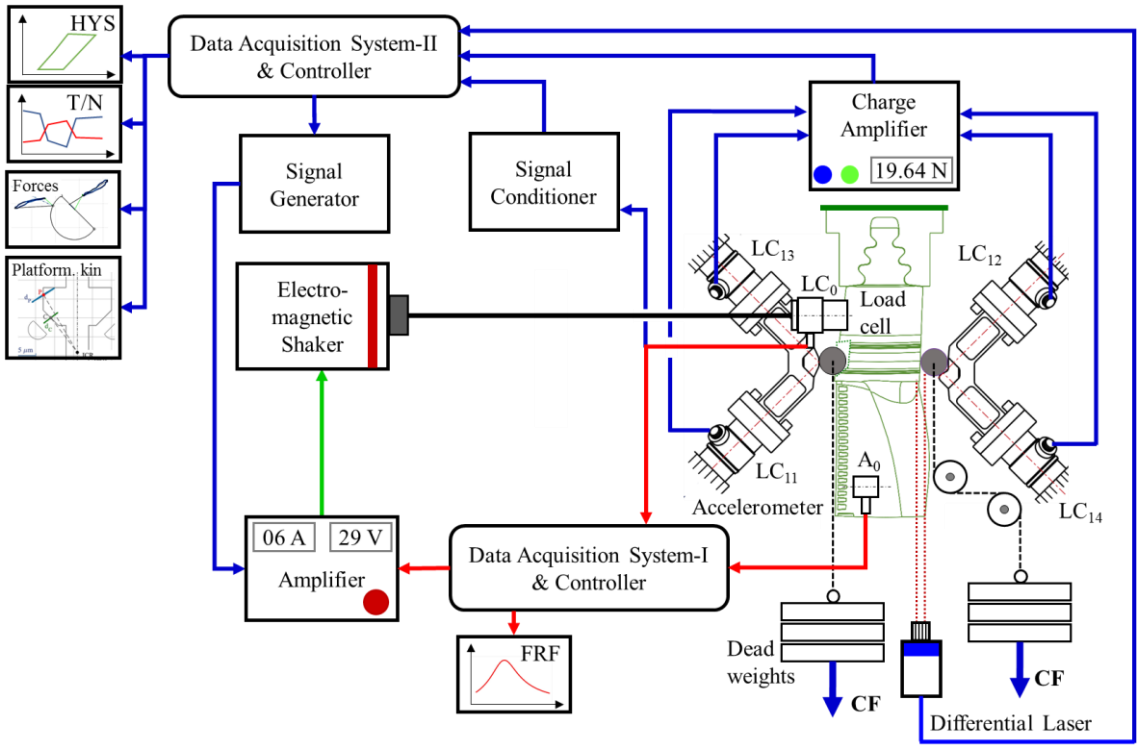

Fig. 2 The Flowchart of the Experimental Framework [15]

3. COMPUTATIONAL BACKGROUND

3.1 Finite Element Model and Governing Equations

The entire test rig had been designed with the help of a computer-aided design software in [15]. In order to obtain system matrices for this study, the blade, the damper and the other auxiliary parts are finely meshed with 3D solid elements as shown in Fig. 3a. The blade and the contact pads (numbered 1 in Fig. 1b) are merged in the finite element model (FEM), since they are tightly bolted in the tests. Similarly, the L-shaped force separator on both sides is also merged with the other contact pad (numbered 2 in Fig. 1b) and load cells. These assumptions are confirmed by preliminary calibration experiments, where the differential laser head recorded zero displacements between contact pads and the respective host structures (either blade or force separator). UPDs are modeled with free-free boundary conditions owing to the fact that they are free to move. The rest of the test rig is considered rigid and excluded in the analyses. Consequently, the model consists of five different bodies. It should be noted that no contact element is imposed to the model in the finite element software. As the boundary conditions, the blade is clamped from the root, while the load cells are fixed from their far ends from the force separator. The Craig-Bampton approach [25] is applied in order to obtain a reduced order model. Physical master nodes, i.e. excitation, static pre-load, response

monitoring, and contact nodes, and 150 modal coordinates are retained as the master degrees-of-freedom (DOF) in the reduction process.

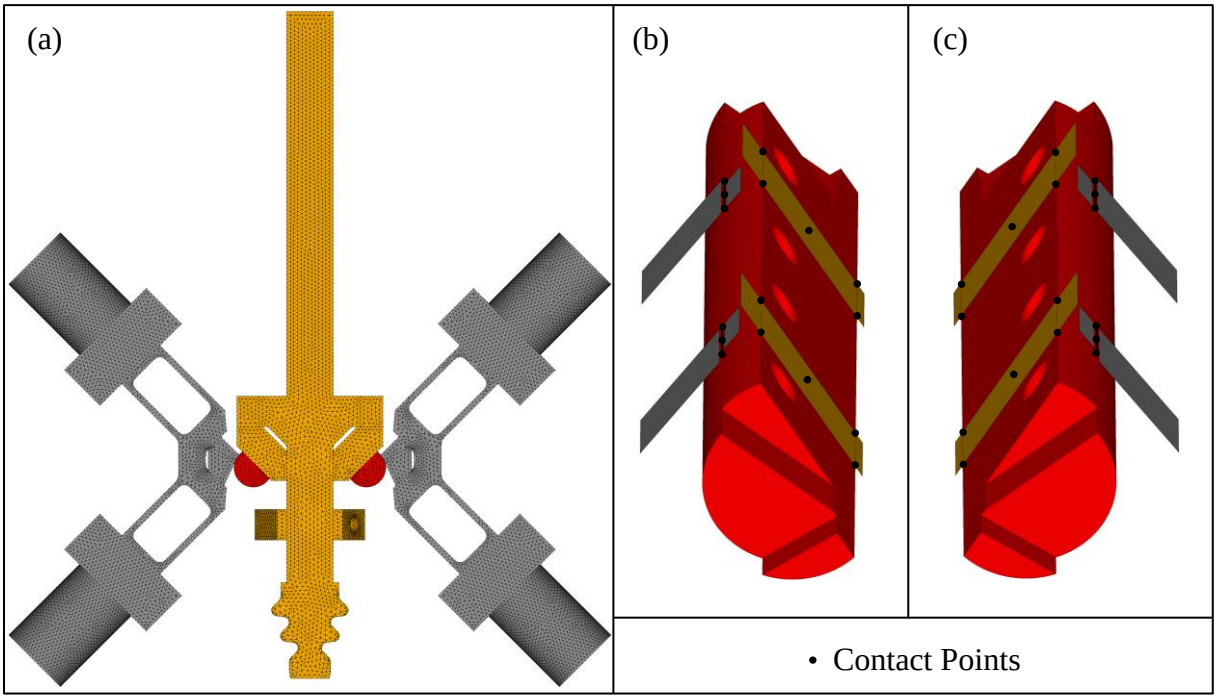

Fig. 3 (a) Finite Element Model of the Structure, (b) Left Damper, (c) Right Damper

Having obtained the system matrices, let us consider the very well-known governing equation of motion for friction-damped systems excited with a harmonic forcing as

$$\mathbf{M}\ddot{\mathbf{q}}+\mathbf{C}\dot{\mathbf{q}}+\mathbf{K}\mathbf{q}+\mathbf{F}_c=\mathbf{F}_{exc}\,. \tag{1}$$

$\mathbf{M}$, $\mathbf{C}$ and $\mathbf{K}$ represent mass, viscous damping and stiffness matrices of the entire test rig, respectively. $\mathbf{q}$, $\mathbf{F}_c$ and $\mathbf{F}_{exc}$ also denote the vector of generalized coordinates, contact forces and excitation forces, respectively, in time domain. The main attention of this study is focused on the steady state solution of the system, where the response, contact forces and excitation forces can be written in terms of their harmonic components as

$$\mathbf{q}=\Re\left(\sum_{h=0}^{H}\hat{\mathbf{q}}^h e^{ih\omega t}\right),\quad \mathbf{F}_c=\Re\left(\sum_{h=0}^{H}\hat{\mathbf{F}}_c^h e^{ih\omega t}\right)\quad\text{and}\quad \mathbf{F}_{exc}=\Re\left(\sum_{h=0}^{H}\hat{\mathbf{F}}_{exc}^h e^{ih\omega t}\right), \tag{2}$$

respectively. Here, $\hat{\mathbf{q}}^h$, $\hat{\mathbf{F}}_c^h$ and $\hat{\mathbf{F}}_{exc}^h$ represent the vector of complex amplitudes for the h^{th} harmonic. H is the number of harmonics considered in the expansion, while i and ω are the unit imaginary number and frequency, respectively. Substitution of Eq. (2) into Eq. (1) gives the nonlinear algebraic set of equations in frequency domain

$$\left(-(h\omega)^2\mathbf{M}+ih\omega\mathbf{C}+\mathbf{K}\right)\hat{\mathbf{q}}^h+\hat{\mathbf{F}}_c^h=\hat{\mathbf{F}}_{exc}^h \qquad (h=0,1,\cdots,H)\,. \tag{3}$$

3.2 Friction Model and Contact Forces

Contact regions are shown in Fig. 3b and Fig. 3c for the dampers located at the left and right, respectively. Each damper has two different contact sides with its neighboring pads. The flat surface of the dampers has an area contact, while a line contact occurs at the cylindrical side. With this type of damper geometry, it has been shown in [16] that the system kinematics mostly provides a micro slip and a full stick motion at the cylindrical and flat side, respectively. Correspondingly, in this study, different contact models are used at each contact interface to be able to better represent the contact conditions.

On the flat sides, the Jenkins element [26], which is shown in Fig. 4a, is used to model the frictional behavior. The number of contact pairs to be used in the final nonlinear analyses is determined with a pre-tuning process, where the effects of different quantities of Jenkins elements used at the flat sides are examined initially in the preliminary nonlinear response analyses. It is concluded that increasing the number of elements does not increase the accuracy of the solutions, since the flat side is already fully stuck. As a result, five particular points are selected per each contact area (see Fig. 3b and Fig. 3c), evenly distributed on the entire surface, with four of them lying at the corners and the last one exactly in the middle.

On the other hand, a micro slip element, which is depicted in Fig. 4b, is utilized for the line contact on the cylindrical side. The micro slip element is basically an array of concatenated macro slip elements. It has been firstly developed for non-conforming contact surfaces in [27] and validated experimentally on UPDs in [28]. Its main principle is to capture the micro slip behavior by splitting the hysteresis cycle into several portions with linear stiffness elements. This idea has also been used in [29, 30] and facilitates the imitation of the micro slip behavior with a simple strategy. In our case, the number of concatenated elements in a single micro slip element is five, and three distinct contact points are chosen on the line contact as shown in Fig. 3b and Fig. 3c. In this way, a total number of 15 macro slip elements are distributed over a relatively small contact line. This enables the computation of micro slip phenomenon with a satisfactory level of accuracy. It is also worth noting that 80 macro slip elements are used in total within the entire model of the structure, where 20 of them are located on the flat sides and the rest on the cylindrical portions.

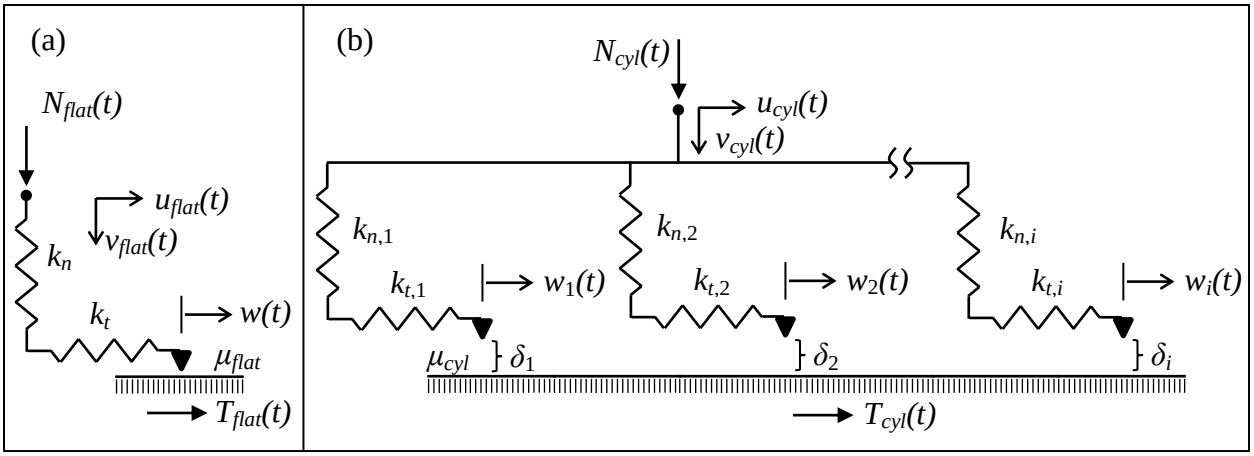

Fig. 4 (a) Macro slip Jenkins Element, (b) Micro slip Array Element

Contact forces for each point of the flat side in the normal, $N_{flat}(t)$, and tangential, $T_{flat}(t)$, directions can be computed for a Jenkins element as follows

$$N_{flat}(t) = \max\left(k_n v_{flat}(t), 0\right) \quad , \quad T_{flat}(t) = \begin{cases} k_t\left[u_{flat}(t) - w(t)\right] & \text{stick state} \\ \mu_{flat} N_{flat}(t)\,\text{sign}\left(\dot{w}(t)\right) & \text{slip state} \\ 0 & \text{lift-off state} \end{cases} . \quad (4)$$

$v_{flat}(t)$ and $u_{flat}(t)$ represent the relative displacements in the normal and tangential directions for the flat surface, while $w(t)$ is the slip motion at the contact points. k_n, and k_t are the contact stiffness values in the normal and tangential directions, respectively. μ_{flat} is the friction coefficient for the flat surface. The numerical values of the contact parameters utilized in this study are determined with a two-step procedure. First, a possible range of values is defined by considering the values extracted in the previous studies where the damper geometry of this work has been manufactured many times using the same material and studied separately [16, 27, 28, 31, 32]. Since there are several factors that may affect the actual values of the contact parameters, an uncertainty band is a typical feature of experimentally determined properties. The range for k_t has been determined as 20-70 N/μm [16, 31, 32], while it has been set at 12-186 N/μm for k_n [31]. The numerical value of μ_{flat} has also been defined with a range of 0.4-0.6 [28, 31, 32]. The final values of the contact elements are then finely tuned in the computational analyses by remaining within the pre-defined experimental range.

On the other hand, since the micro slip element is an array of the macro slip elements, the contact force for each point on the cylindrical side is the summation of the contribution of each sub-element [28]:

$$N_{cyl}(t)=\sum_{i=1}^{5}N_i(t) \quad , \qquad N_i(t)=\max\left(k_{n,i}\left(v_{cyl}(t)-\delta_i\right),0\right) . \tag{5}$$

$$T_{cyl}(t)=\sum_{i=1}^{5}T_i(t) \quad , \qquad T_i(t)=\begin{cases} k_{t,i}\left[u_{cyl}(t)-w_i(t)\right] & \text{stick state} \\ \mu_{cyl}N_i(t)\text{sign}\left(\dot{w}_i(t)\right) & \text{slip state} \\ 0 & \text{lift-off state} \end{cases} . \tag{6}$$

It should be noted that there is an additional pre-defined gap, δ_i, in the normal force expression of each sub-element. The other notations are kept the same for clarity. The global properties of the micro slip contact element for the cylinder-on-flat surfaces, $\sum_i k_{t,i}$, $\sum_i k_{n,i}$ and μ_{cyl}, have also been previously extracted in [16, 27, 28, 31, 32]. $\sum_i k_{t,i}$ has been defined in a range of 16-44 N/μm [16, 28, 31, 32], while the value of $\sum_i k_{n,i}$ has been larger as 260 [28] N/μm. μ_{cyl} has also been defined in the range of 0.4-0.65 [16, 27, 28, 32]. The subdivision of the global stiffness values into each sub-element contributions $k_{t,i}$, $k_{n,i}$ and the gap vector values δ_i have been determined according to the procedure described in [27, 28]. All relevant details on the micro slip element can be found in [28].

It is worth mentioning that the slip motion, *w(t)*, is an uncertain parameter in contact elements during the stick state. To overcome this difficulty, a predictor-corrector method [33] is used in the computation of contact forces. In this approach, the slider is initially assumed in the stick state with a predicted slip value. Under this condition, if the estimated friction force is less than the limit value, $\mu N(t)$, the assumption holds. Otherwise, the friction force and the slip motion are correspondingly corrected. In addition, the complex amplitudes of the contact forces are obtained by utilizing the Alternating Frequency/Time approach [34], which requires successive transformations from frequency domain to time domain and vice versa. The exact details of the methods are not given here for brevity and more interested readers may refer to original studies.

3.3 Non-Unique Contact Forces and Dynamic Response Variability with Boundaries

Non-uniqueness of the friction forces is a phenomenon that has been studied previously both in the contact mechanics [11-13] and in the turbomachinery [14-22] communities. In this study, no contribution is made to its theoretical background, and its detailed investigation is

out of scope here. Nevertheless, a very brief recap on the uncertainty phenomenon and its outcomes is presented in this section for the sake of completeness. Interested readers may refer to [14, 18, 21, 22] for a more detailed explanation about its fundamental physics and the applications with different case studies.

As a rule of thumb, the Coulomb's law states that the friction force in the tangential direction must be lower than a limit value for a fully stuck contact point, i.e. $|T(t)| < \mu N(t)$. This fact creates an uncertainty in the static component of the tangential force, T^0, where a variability range can be defined as shown in Fig. 5. In this range, an infinite number of $T(t)$, whose dynamic components are totally identical, is possible with different T^0 values. This means that the tangential force of fully stuck points is non-unique. It should be noted that the uncertainty exists only for fully stuck elements, since the friction force of slipping contacts are characterized by a unique value. i.e. $|T(t)| = \mu N(t)$.

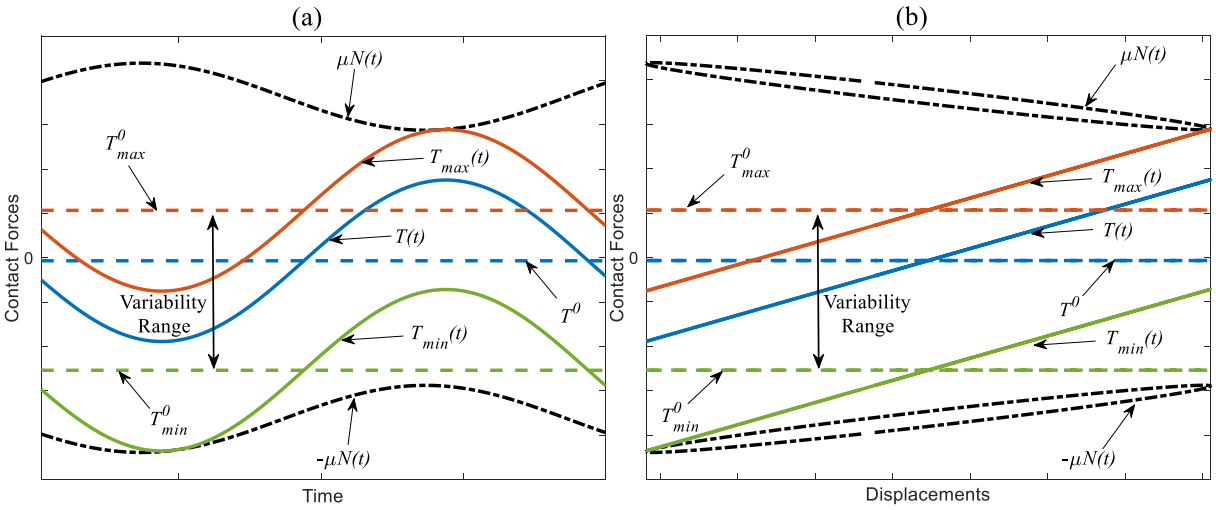

Fig. 5 Contact Forces with the Variability Range for a Fully Stuck Point: (a) Time Histories, (b) Hysteresis Cycles [21]

Non-unique tangential forces may cause the system to have a variable dynamic kinematics under the same nominal conditions. To mathematically illustrate this situation, consider a frictional structure under an external excitation together with a pre-load. In this condition, the system matrices ($\mathbf{M}$, $\mathbf{C}$ and $\mathbf{K}$) and the forcing parameters ($\hat{\mathbf{F}}_{exc}^{h}$, h and ω) are already prescribed in Eq. (3) from which the dynamic behavior can be determined; however, the non-uniqueness of the static friction force imposes that there exist multiple version of $\hat{\mathbf{F}}_{c}^{0}$ that is capable of satisfying the equilibrium in Eq. (3). This physically corresponds to different static force balance equilibria achieved in the system under the same nominal conditions. As a

result, the response of the system, $\hat{\mathbf{q}}^h$, becomes non-unique due to the coupling present in Eq. (3). It is worth mentioning that the response variability can only be obtained under a partial slip condition. Moreover, there should be an interaction between the tangential and the normal forces of different contact regions, typically referred to as cross coupling [21], as non-unique tangential forces of a fully stuck point will change the normal forces of other slipping pairs. This, in turn, provides a variable dynamic characteristic in the system even if all the inputs are nominally identical. More information about the mathematical and physical explanation of the uncertainty phenomenon can be found in [21, 22]. All the details are not given here for brevity.

The variability of the response makes its boundaries essential to be computed, from an engineering point of view. In this study, the systematic method developed very recently in [22] is utilized to determine the response limits. It is based on an optimization algorithm that minimizes the system's loss factor, η, with a nonlinear constraint obtained with the Harmonic Balance Method (HBM) as

$$\begin{array}{ll} \text{minimize} & \eta \\ \text{with respect to} & [\hat{\mathbf{q}}^{\mathrm{T}}, \mathbf{m}^{\mathrm{T}}]^{\mathrm{T}} \\ \text{subject to} & \mathbf{R} = \mathbf{0} \end{array} . \tag{7}$$

The loss factor is the ultimate parameter that determines the damping capability of the system [35, 36] and it can be calculated as

$$\eta = \frac{\Delta W_{dis}}{2\pi U_{pot}} . \tag{8}$$

ΔW_{dis} and U_{pot} are the system's total dissipated energy and the maximum potential energy corresponding to the response amplitude levels, respectively. The optimization algorithm makes use of an additional unknown parameter, $\mathbf{m}$. This is a vector of multiplier coefficients and its elements represent the ratio between the initial estimate of the tangential force and the Coulomb's limit force for each contact element in the predictor-corrector scheme

$$T_i(t_{ini}) = m_i \times \mu N_i(t_{ini}) \qquad \left(i = 1, 2, \cdots, N_c\right), \tag{9}$$

where N_c is the number of contact elements in the system. $\mathbf{R}$ denotes the residual of the nonlinear set of algebraic equations (see Eq.(3)) and it can be obtained as

$$\mathbf{R} = \hat{\mathbf{q}}^h + \boldsymbol{\alpha}^h \left(\hat{\mathbf{F}}_c^h - \hat{\mathbf{F}}_{exc}^h - \mathbf{K}_c \hat{\mathbf{q}}^h \right) \quad (h = 0,1,\cdots,H), \tag{10}$$

where $\boldsymbol{\alpha}^h = \left(-(h\omega)^2 \mathbf{M} + ih\omega \mathbf{C} + \mathbf{K}_{stuck} \right)^{-1}$ and $\mathbf{K}_c = \mathbf{K}_{stuck} - \mathbf{K}$, being $\mathbf{K}_{stuck}$ is the stiffness matrix of the fully stuck linear system.

It should be noted that Eq. (7) determines the upper boundary, since the damping in the system is minimized. The lower boundary can be computed with a similar procedure but by using the negative of the loss factor as follows

$$\begin{array}{ll} \text{minimize} & -\eta \\ \text{with respect to} & [\hat{\mathbf{q}}^{\mathrm{T}}, \mathbf{m}^{\mathrm{T}}]^{\mathrm{T}} \\ \text{subject to} & \mathbf{R} = \mathbf{0} \end{array} . \tag{11}$$

The linear and nonlinear DOFs are also partitioned in the solution scheme [36] in order to decrease the computational time. In this study, the interior-point method [37, 38] with *fmincon* function built in MATLAB is utilized as the optimization algorithm. All the numerical gradients are numerically calculated by using the forward finite difference method. The detailed information on the whole solution process can also be found in [22].

4. RESULTS

4.1 Linear Dynamic Characteristics of the Blade

The experimental linear behavior of the blade without engaged dampers can be used to extract the modal properties, i.e. natural frequency and damping ratio. These measured values are utilized to tune the linear model, before performing the experimental-numerical comparison on the nonlinear analyses.

The natural frequency of the blade may be severely affected by boundary conditions. Even though the blade root can be perfectly constrained in the FEM, the same condition may not be valid in laboratory conditions even if very large clamping forces are applied. Hence, a sensitivity analysis in the FEM is firstly performed on the root boundary conditions in order to ensure a good match between the first natural frequency of the blade obtained numerically and its experimental counterpart. The natural frequency of the blade for the well-separated first bending mode is measured at 410 Hz in the experiments, and it is afterwards tuned to the

same value in the numerical analyses with the sensitivity study. Fig. 6a depicts the interested mode shape at 410 Hz.

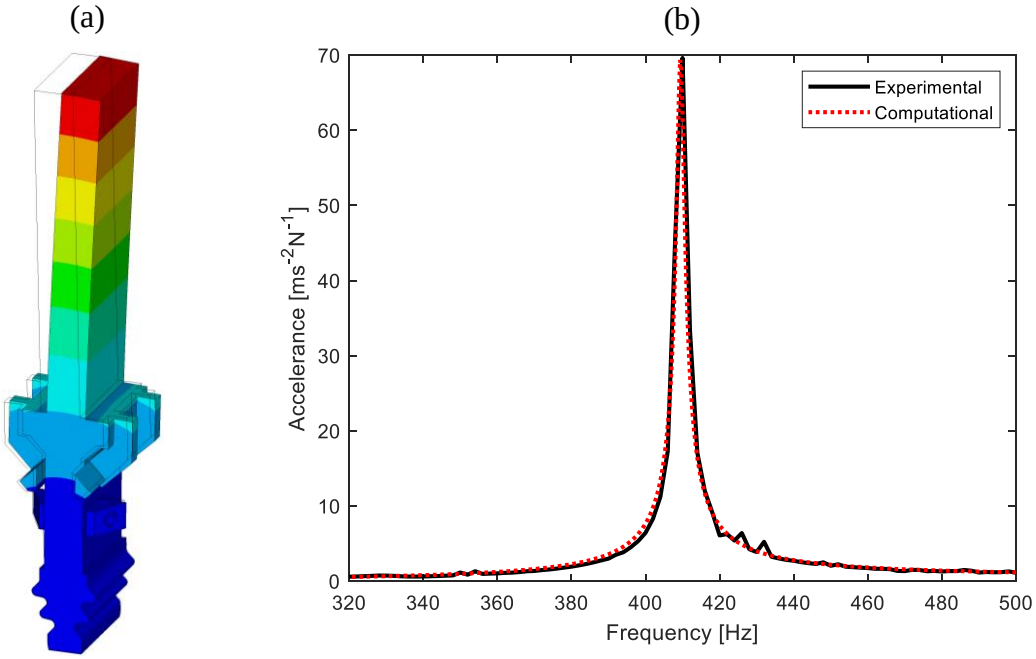

Fig. 6 (a) The First Lateral Bending Mode Shape of the Blade at 410 Hz (b) Linear Response of the Blade Tip without Under-platform Dampers

Fig. 6b shows the experimental and computational linear responses of the blade without UPDs around the first resonance region. The accelerance amplitude of the blade tip is given. The responses almost overlap, thus providing an evidence of the fact that the linear behavior of the blade in the numerical model represents the real working conditions with a negligible amount of deviation. It should be noted that this verification is a key step that needs to be performed prior to nonlinear analyses; because, it prevents a potential artificial stiffness contribution from the root, which may introduce errors in the subsequent contact stiffness tuning at the platform-damper contact. It is also worth mentioning that although the damping ratio of the stand-alone blade model is estimated from the experimental result, the one corresponding to the entire system and used in the nonlinear analyses is finely tuned after engaging the UPDs in the next section.

4.2 Nonlinear Behavior of the Blade Coupled with UPDs

Dynamic response variability of the blade with UPDs is both computationally and experimentally investigated with various excitation levels (1-100 N) and three different pre-loads (2.6 kg, 4.6 kg and 6.6 kg). Before the nonlinear response computations, the linear damping ratio and contact parameters are calibrated in the numerical model.

A proportional damping ratio for the entire linear system with UPDs is used. Its value is determined by the experimental results obtained with the lowest excitation force level, which gives the closest configuration to the fully stuck linear system. The damping ratio value is set to 0.8% and kept constant for the all analyses.

A preliminary analysis is performed for the characterization of contact elements in the model. First, the Jenkins element is used on both sides of the damper (cylinder-on-flat and flat-on-flat contacts alike). However, the accuracy of the experimental-numerical match was deemed not satisfactory, especially for low excitation levels. One hypothesis to explain this discrepancy is the absence of a contact model capable of capturing the micro slip behavior at the cylinder-on-flat contact. In fact, a series of simple Jenkins elements evenly distributed along the line contact observed at the cylinder-on-flat side cannot capture partial slip phenomena, especially for a bending mode. Then, the micro slip array element [27, 28] is utilized at the cylindrical side, while the Jenkins elements are still kept at the fully stuck flat side. This new configuration significantly improves the experimental-numerical match.

The contact parameters are tuned to three sets of values, one for each pre-load case. This approach is relevant, since the contact pressure on the frictional surfaces in the experiments is different for each pre-load. A two-step procedure is followed to tune the contact parameters. First, the pre-defined experimental range, which is given in Section 3.2, is taken as a starting reference point. Then, these values are finely tuned to optimize the experimental-numerical match, keeping into account the variability due to the different static conditions. The final values are given in Table 1 and kept constant during the analyses. A further proof of the model consistency is that contact stiffness values tend to increase with increasing pre-load values, i.e. contact pressure, as observed in [31] and demonstrated in [40, 41].

Table 1 Contact Parameter Sets for Different Cases of Pre-load

Applied Pre-load	Damper Side	Tangential Stiffness [N/μm]	Normal Stiffness [N/μm]	Coefficient of Friction
1st set for 2.6 kg	Flat	20	50	0.6
	Cylindrical	45	260	0.4
2nd set for 4.6 kg	Flat	25	65	0.6
	Cylindrical	45	260	0.4
3rd set for 6.6 kg	Flat	35	75	0.6
	Cylindrical	35	260	0.4

It should be highlighted once again that the main goal of this study is not to perform additional tests to experimentally extract the contact parameters used in the computational

analyses. The calibration and validation of these properties has already been deeply investigated and presented in the previous studies for the damper geometry utilized in this work [16, 27, 28, 31, 32]. Here, the final values are tuned after a considerable amount of effort, so that they remain within the ranges demonstrated previously and they represent the most optimized ones that give a satisfactory level of accuracy for the comparison of experimental-numerical match. In the next parts, the results are presented and discussed in three different sub-sections. In the first one, the largest amount of data is collected and a thorough comparison is performed with 4.6 kg pre-load case. The numerical method is then challenged with further experimental data obtained at 6.6 kg and 2.6 kg of pre-load cases in the second and the third sections, respectively.

4.2.1 Multiple Nonlinear Responses with the Variability Range and Non-Unique Contact Forces for 4.6 kg Pre-Load Cases

There may be various parameters that affect the repeatability of the response in frictional structures, as mentioned previously in the introduction. It is always challenging to eliminate all factors that are out of user control. One of the relevant approaches to identify the underlying reason of the non-repeatability is to keep macro scale testing conditions as similar as possible and to repeat the experiments under the same nominal conditions. Then, the only variable parameter in the different repetitions gives an insight on the cause of the variability. This idea is applied also in the current work. Before presenting the response variability, it is first intended to demonstrate the main factor of non-repeatable data obtained in our experiments. For this purpose, a purposely defined strategy is followed [16]. In particular, a first set of the experiments is performed with an increasing order of excitations from 1 N to 100 N; and then in the second set, the same logic is applied but with the opposite direction decreasing back to 1 N from 100 N. In all the tests, the pre-load is kept constant at 4.6 kg. All sweeps performed with 20 N excitation are then collected and studied.

Fig. 7 and Fig. 8 show the contact forces measured on the right and left dampers, respectively, in four different runs with 20 N excitation and 4.6 kg pre-load. Tangential and normal forces are shown in one full vibration cycle at the corresponding resonance frequencies for both flat and cylindrical sides. It is seen that the contact forces of the first (before 100 N excitation) and second (after 100 N excitation) sets closely gather within themselves, but with an offset from each other. Dynamic parts of contact forces oscillate around non-unique static components in different runs. This is an indication of different static balances achieved in each set, although the applied pre-load is nominally same. It can be said that the micro

conditions in the frictional interfaces is blindly modified from a macro scale environment with the followed strategy, by keeping all user-controlled inputs identical. As mentioned in Section 3.3, the uncertainty phenomenon provides the system to have a non-unique static force balance pattern, even if all the inputs are nominally same. As a result, it can be inferred that the response variability observed in our experiments is due to the non-uniqueness of friction forces, since the contact forces balance the equilibria with different static components in each run.

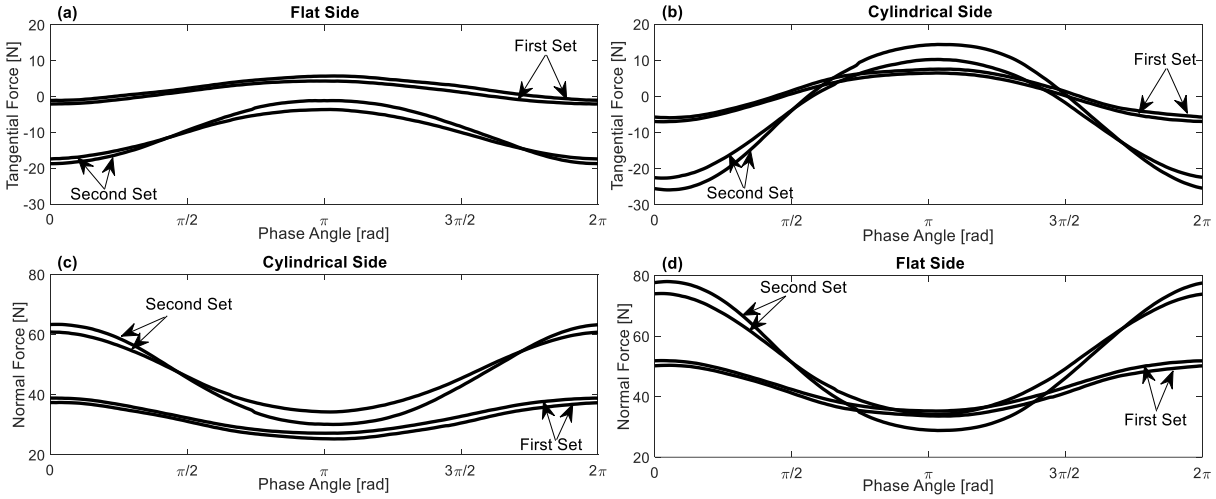

Fig. 7 Experimental Contact Forces on the Right Damper for 20 N Excitation Case in one Full Vibration Cycle at the Corresponding Resonance Frequencies

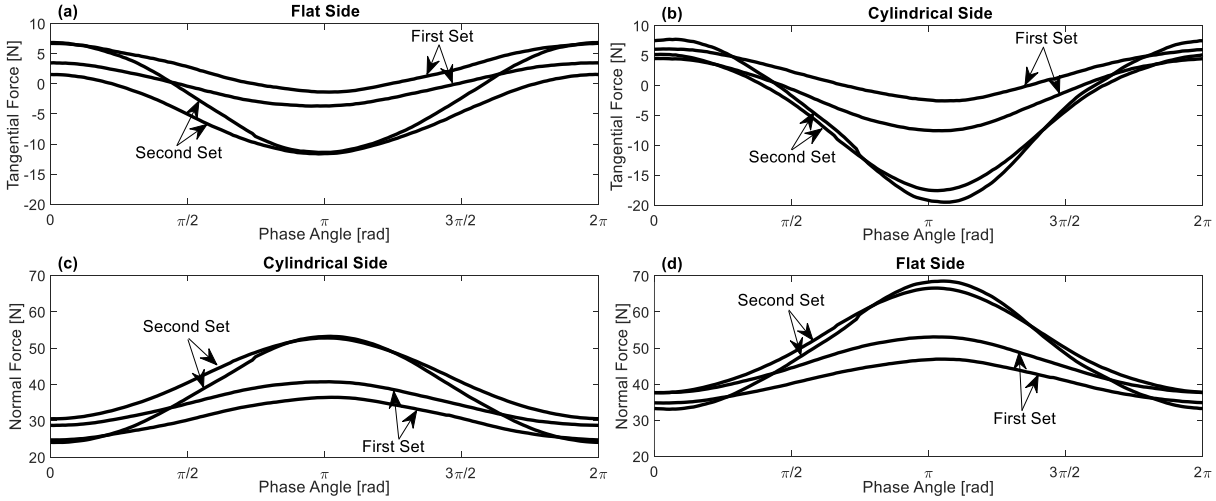

Fig. 8 Experimental Contact Forces on the Left Damper for 20 N Excitation Case in one Full Vibration Cycle at the Corresponding Resonance Frequencies

Fig. 9 depicts the complete picture of the nonlinear response data for the pre-load with 4.6 kg. Normalized response amplitudes are grouped and presented in six different sub-plots with respect to the excitation. For instance, Fig. 9a shows eight different responses corresponding

to 1 N excitation, where three of them (solid black curves) are measured in the experiments, and the rest is obtained in the computational simulations. The experiments for each excitation set are performed under the same nominal conditions by keeping all the user-controlled inputs identical. The response variability obtained in the experiments cannot be explained with abrasion or wear, since the test durations are considerably short. Instead, as mentioned above, different static force equilibria corresponding to each run induce a change in the equivalent stiffness and damping of the frictional contacts, leading to multiple responses for the same nominal conditions. On the computational side, analyses are performed in two different ways. The first one uses a nonlinear solver with the HBM, developed in MATLAB, and calculates the steady state vibration amplitude of the system. This gives one of the multiple responses (dotted red curves) in each analysis shown in Fig. 9a-f. The variation of the steady state response here is provided with different initial guess values of the static tangential forces during the computation of contact forces within the AFT algorithm. The second way utilizes the optimization algorithm proposed in [22] and estimates the boundaries (dash-dotted green curves), which is the main goal of the current study. The loss factor of the system is used as the objective function in the optimization. The upper and lower limits are predicted with the minimum and maximum values of the loss factor in two different analyses, respectively.

The results show that the experimental limits of the variability range as well as the nonlinear dynamics of the blade with UPDs are satisfactorily captured by the numerically estimated boundaries and multiple responses, respectively. This verifies the adequacy of the optimization method proposed in [22] to predict the response boundaries. A minor deviation between experimental and computational results is visible in some cases, i.e. the 100 N excitation shown in Fig. 9f. The 100 N excitation case is the one where the nonlinearity is very high due to the large slip. This probably raises some additional issues, which take place in the experiments, but cannot be captured in the numerical model. One possible explanation is that the effect of the shaker stinger on the system becomes dominant in the experiments with the largest excitation, while the stinger-system interaction is not included in the model. It should be noted that the normalized experimental response has a trend for the cases from 1 N to 80 N, where it softens and decreases with increasing excitation. However, experimental results with 100 N do not comply with this observation. It can be observed that an additional stiffness contribution is present, potentially introduced by the shaker stinger, while the normalized computational response continues to soften since no additional stiffening effect is modeled.

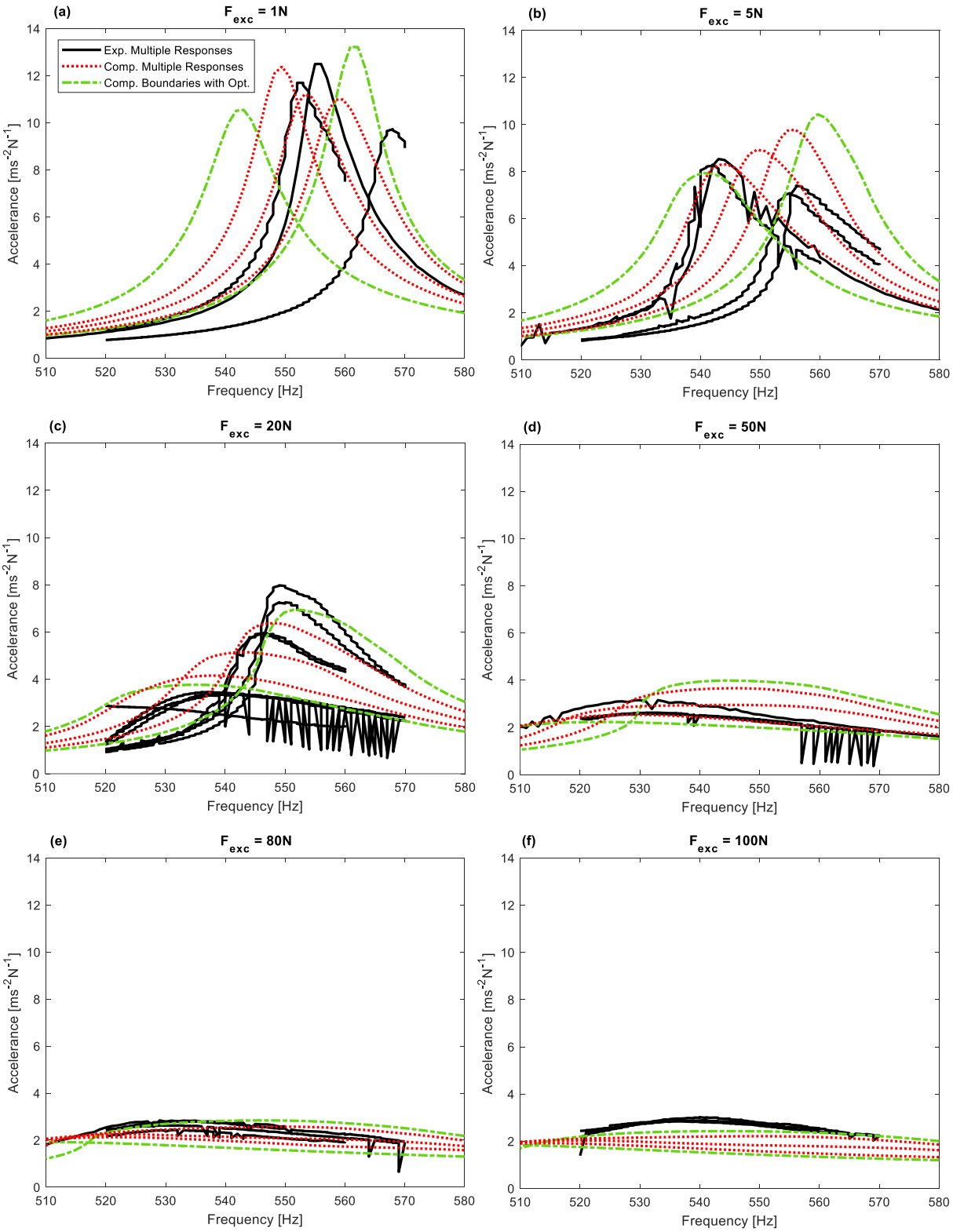

Fig. 9 Nonlinear Response Amplitude of the Blade Tip for Different Excitation Levels with 4.6 kg Pre-Load

It should also be noted that some of the experimental results, especially those in Fig. 9b-d, display an oscillating or *jiggling* trend, i.e. sudden amplitude changes occur at consecutive frequency steps. This is caused by a limit in the shaker force controller, which sometimes

struggles to keep the force amplitude at the predefined constant value for some specific frequencies. Nevertheless, the response behavior is apparent and this problem does not affect the results readability. Another observation is that the variability range is larger for lower excitation cases, while it shrinks with increasing levels of forcing. This can be considered as the second proof of the fact that the response variability in the experiments is mainly due to the non-uniqueness of friction forces. This observation is perfectly consistent with the theoretical hypothesis which defines the non-uniqueness of the solution as a phenomenon that arises from fully stuck points. Once the amount of slip increases in the system, the dynamic behavior converges towards a unique response and the variability range disappears with the gross slip. If there was one another factor that is dominant on the non-repeatability of the response in the experiments, it would have affected the data sharply for higher excitation cases, as well. This can also be illustrated more intuitively by directly comparing the resonance amplitudes with respect to the increasing excitation levels, as shown with the corresponding variability range in Fig. 10.

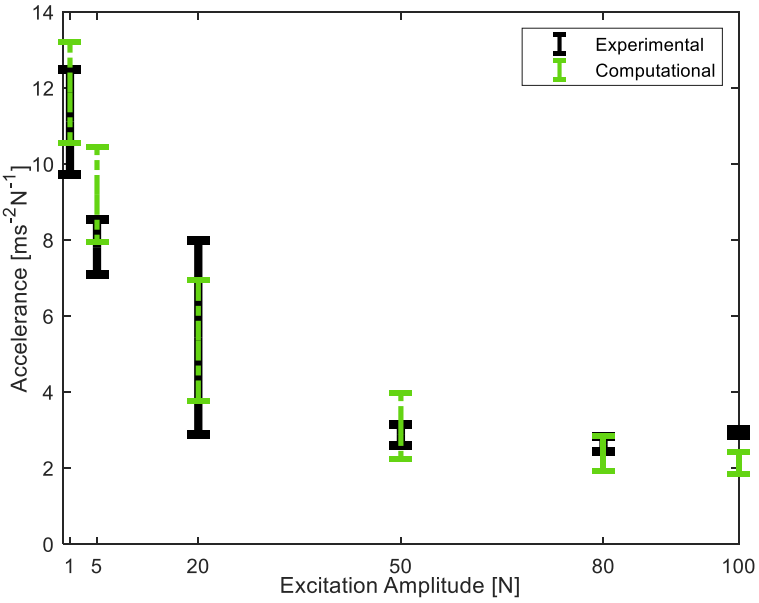

Fig. 10 The Variability Range of Resonance Response Amplitudes for Different Excitation Levels with 4.6 kg Pre-Load

The inherent kinematics of the response variability can be understood better with the contact forces, which is one another valuable output of the current test rig. It is worth first mentioning that the experiments of the current work have been previously performed in [16] to investigate mainly the dissipation capability of the under-platform dampers; hence, the contact force signals are recorded only for the frequency steps across the resonance to be able to limit the size of the time data collected. During the sweep, the recording of the signals is activated just

a few frequency steps before the resonance, whose values are approximately estimated from previous experiments; and then it is stopped after the resonance is surpassed. Since the main attention of the tests has not been focused directly on the uncertainty phenomenon, there is a lack of multiple contact force data for a fixed frequency at a prescribed excitation level and pre-load; hence, one sample of contact forces will be given in the following experimental results. Nevertheless, this condition can still be considered sufficient to make a comparison between experimentally and computationally obtained contact forces, since the main goal here is to numerically capture the boundaries of the variability range in which there is at least one experimental data. It should also be mentioned that recorded time signals are found consistent and repeatable across a single resonance, but the details about the post-processing are not shown here for brevity.

Contact forces are measured for the majority of investigated cases, but two of them, 80 N and 20 N excitation cases, are presented in detail here. These cases are intentionally selected to investigate different kinematics. They serve as demonstrators, as the variability is lower in the former, while it is much larger in the latter. Another motivation for selecting these cases is also that the experimental and computational results of the response match quite accurately and this enables a close comparison of contact force results.

4.2.1.1 Contact Forces for 80N Excitation Case

The uncertainty phenomenon is directly related to the contact conditions, since the non-uniqueness of tangential forces occurs only in fully stuck points. Hence, first, the contact status on the frictional interfaces is investigated, particularly around the resonance frequency (ω = 529 Hz).

Fig. 11 shows the proportion of contact forces on each side of the right damper for one full vibration cycle. In addition to the experimental result, computational ones are also given. It can be deduced from Fig. 11a that the force ratio (T/N) at the flat side exhibits a behavior that is close to a sinusoidal motion. This indicates that gross slip is never achieved, which is a case also verified computationally by monitoring the status of the contact points. A great majority of the contact elements on the flat side are fully stuck; while a few ones have a stick-slip contact condition, but largely dominated by the stuck state. On the other hand, Fig. 11b shows that a gross slip occurs on the cylindrical side, since the force ratio becomes equal to the coefficient of friction, i.e. $T/N = \mu$, in some portions of the cycle, as indicated by the labels in Fig. 11b. This behavior is clearly visible in the computational analyses with a perfect straight

line, while it has a more rounded shape in the experimental counterpart. Nevertheless, the transition between the stick and slip states is visible for both cases and is further highlighted in Fig. 11b through the use of red and black dots for the computational and experimental results, respectively.

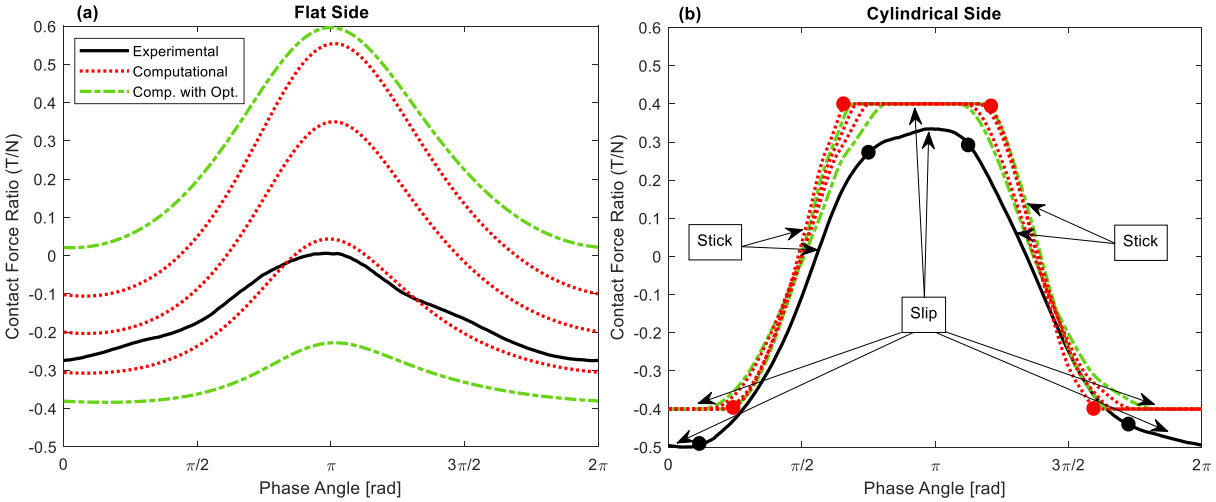

Fig. 11 Contact Force Ratio of 80 N Excitation Case in one Full Vibration Cycle at ω = 529 Hz for the Right Damper: (a) Flat Side, (b) Cylindrical Side

Fig. 12a and Fig. 12b show the tangential forces on the right damper for both flat and cylindrical sides, respectively. This set of forces corresponds to the one used to produce the results in Fig. 11. Since the contact surfaces on the flat side are in the stick condition, the tangential force on this side is non-unique as shown in Fig. 12a. It is also clear in Fig. 12a that the limit forces obtained computationally with the optimization algorithm successfully bound the variability range in which the experimental result is also present. This is one of the key results of the current study and proves the effectiveness of the optimization method once more. Focusing the tangential forces on the cylindrical side in Fig. 12b, it is known that the slip condition significantly lowers the uncertainty caused by the non-uniqueness of tangential forces on this side. However, variability is still visible. This is explained by the fact that the forces at the cylindrical and flat contacts are coupled, i.e. the uncertainty at the flat side influences the variability at the cylindrical side. Hence, the tangential force on the cylindrical side also varies due to different force balances, as shown in Fig. 12b. The curves follow a common pattern and share a similar behavior.

The damper induced cross-coupling (see Fig. 1c) has an important impact on the behavior of normal forces; it can be observed how the normal force on one side is mostly affected by the tangential force on the opposite side. Fig. 12c depicts the normal forces on the cylindrical side, where a variability range is seen, as expected, due to the uncertainty of tangential forces

on the flat side. This variability is also bounded by the limit forces obtained with the optimization algorithm. Fig. 12d shows the normal forces on the flat side, which follow a similar pattern to that of the tangential forces on the cylindrical side shown in Fig. 12b. It can also be noticed in the all results that experimental results are successfully captured by one of the computationally obtained curves, both in amplitude and in overall trend.

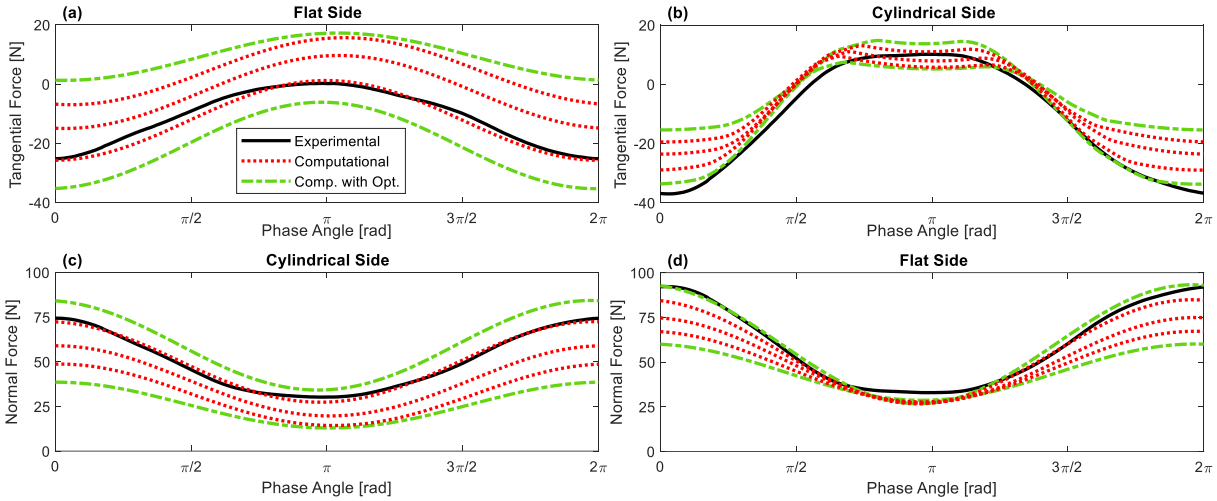

Fig. 12 Contact Forces on the Right Damper for 80 N Excitation Case at ω = 529 Hz

In Fig. 13, the contact forces produced at the left damper contacts are shown. The trends are the same as those shown for the right damper. The variability range of non-unique tangential forces for the fully stuck flat side is successfully predicted with the method proposed in [22]. The experimental results are computationally obtained with a high accuracy. All of these observations not only show the superior performance of the method, but also support the fact that the dynamic response variability is created by the uncertainty related to the non-uniqueness of tangential forces.

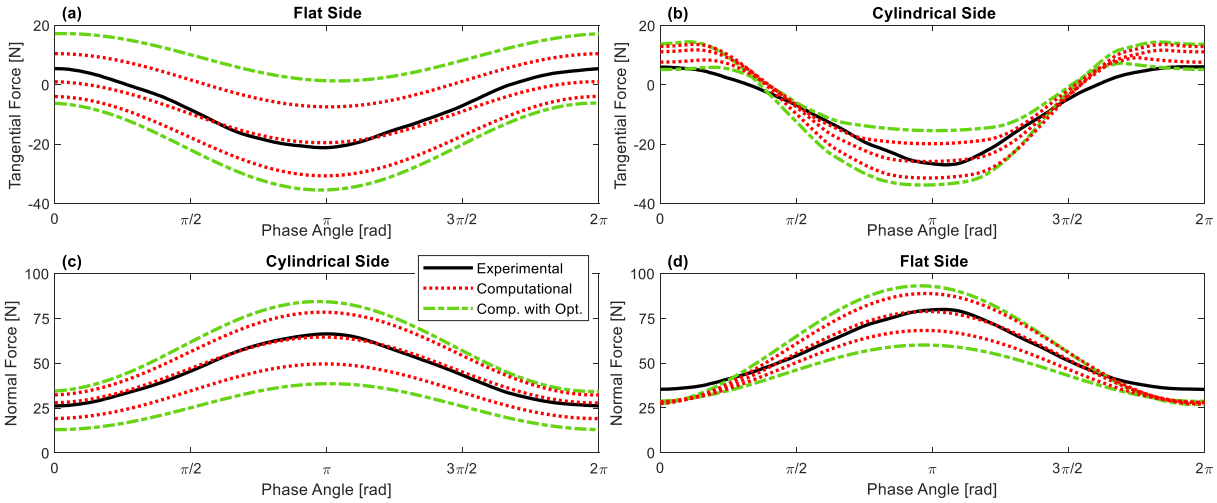

Fig. 13 Contact Forces on the Left Damper for 80 N Excitation Case at ω = 529 Hz

4.2.1.2 Contact Forces for 20 N Excitation Case

This case study has a larger variability range than the 80 N excitation (see Fig. 9). In order to investigate the limiting cases, the contact forces are studied at the resonance of the two boundaries of the variability range, i.e. at ω = 549 Hz and at ω = 536 Hz.

First, the contact status is investigated once again, in order to better interpret the force results. In this case, the relative displacement between the damper and the blade is measured on one side in each recording, by using a differential laser. Fig. 14 illustrates the hysteresis cycles with the corresponding tangential force and relative displacements for the contacts on the left damper. Fig. 14a shows that the flat side is under a fully stuck condition, while the energy is dissipated with a micro slip on the cylindrical side as shown in Fig. 14b. It should be noted that the amplitude of the relative displacement is so small, so the laser struggles to measure it smoothly. Hence, a zigzag behavior and unrealistic vertical lines are seen in the experiments. Nevertheless, the results give a clear indication on the contact status and the computational and experimental results share the same order of magnitude both in terms of force and displacement range.

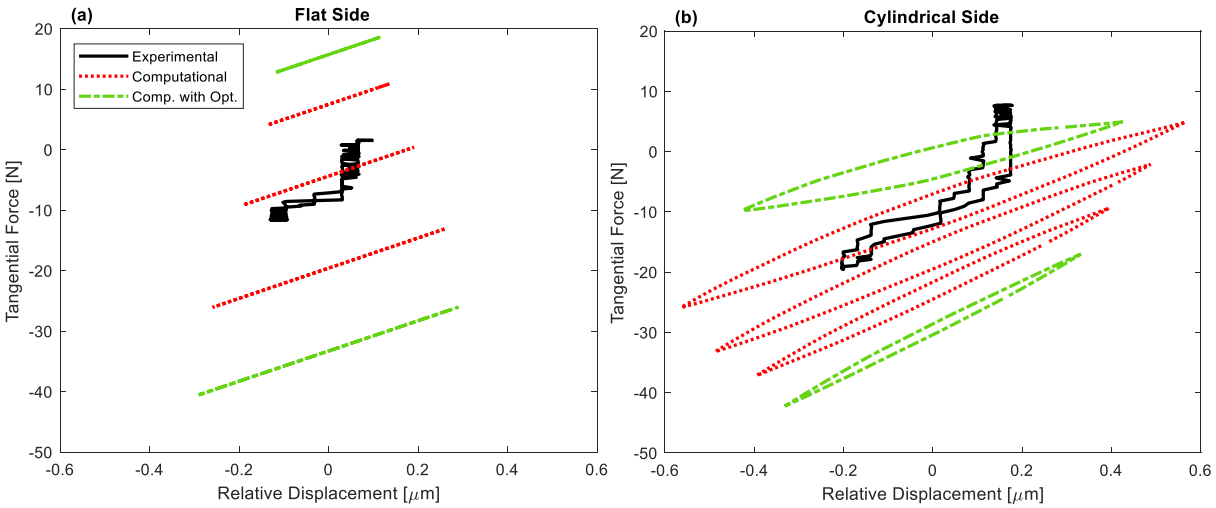

Fig. 14 Hysteresis Cycles of 20 N Excitation Case for the Left Damper: (a) Flat Side, ω = 549 Hz, (b) Cylindrical Side, ω = 544 Hz

Since the flat side is fully stuck, the variability range of the non-unique tangential forces is clearly visible in Fig. 14a. The range is again bounded by the forces obtained with the optimization method. On the cylindrical side (see Fig. 14b), it is very interesting to note that the static component of the forces is bounded by the optimization method, but the same phenomenon is not valid for the dynamic component and the amount of dissipated energy (internal area of the cycles). This is relevant; because, the optimization algorithm does not

utilize the dissipated energy itself, but the loss factor, which is the proportion of the dissipated energy over the stored energy, as the objective function to minimize. This also explains the evidence shown in Fig. 9c where some of the computationally obtained multiple responses (dotted red curves), which stay within the upper and lower limits (dash-dotted green curves), can exceed the boundaries at some specific frequencies.

Fig. 15 shows the contact forces measured at ω = 549 Hz on the left damper. In this case, the non-uniqueness uncertainty and the damper induced cross coupling create a larger variability range than the previous results in Section 4.2.1.1, in the tangential force of the flat side (see Fig. 15a) and in the normal force of the cylindrical side (see Fig. 15c), respectively. This is expected; as gross slip is achieved in the previous case, while a micro slip is dominant here. Hence, the behavior of the nonlinear response in the former was closer to a unique one than the latter. Regardless of the situation, the optimization method still works very-well and bounds the range including the experimental results, in Fig. 15a and Fig. 15c. The experimental and computational results match quite accurately in Fig. 15b and Fig. 15d, as well.

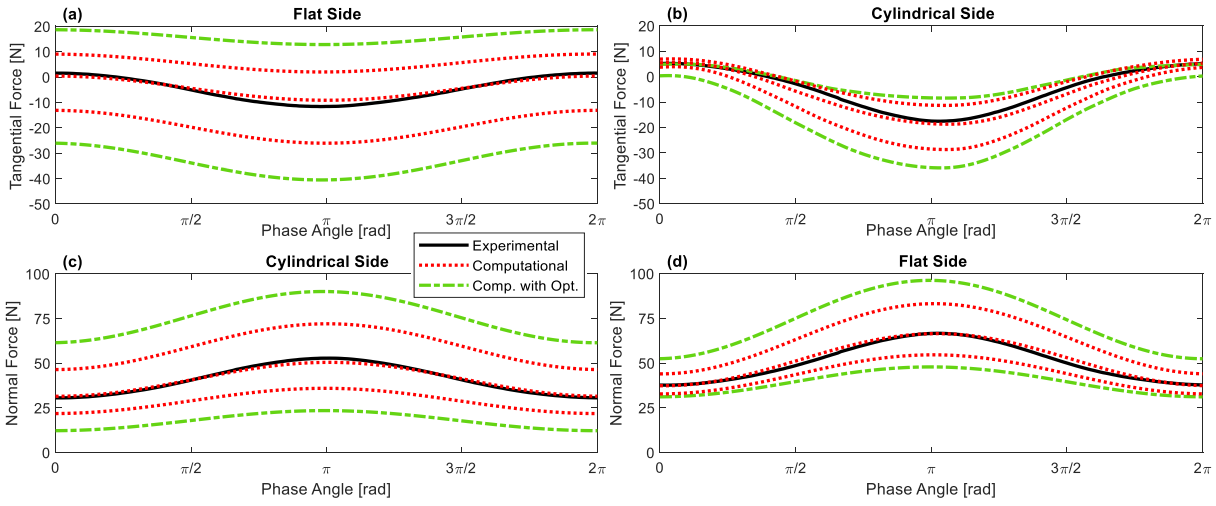

Fig. 15 Contact Forces on the Left Damper for 20 N Excitation Case at ω = 549 Hz

Fig. 16 depicts the contact forces for the same conditions, but on the right damper. As expected, all the results show a coherent and a repetitive behavior. It should also be noted that, some of the computational tangential forces shown in Fig. 16b have larger dynamic amplitudes than those predicted by the optimization algorithm. This is another example of the previous observation that the limits predicted by the optimization algorithm may be out-bounded by some of the nonlinear responses for limited portions of the vibration period at specific frequencies.

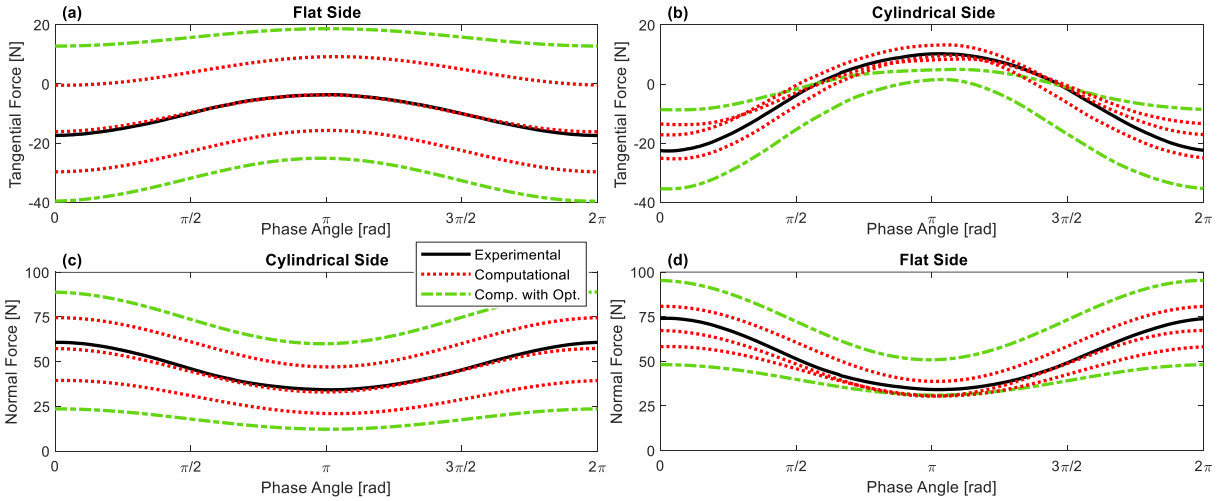

Fig. 16 Contact Forces on the Right Damper for 20 N Excitation Case at ω = 549 Hz

The contact forces are also investigated at the resonance of the lower limit (ω = 536 Hz), to check whether the method will be able to capture the range of variability. Fig. 17 and Fig. 18 illustrate the contact forces on the left and the right dampers, respectively. The results show the outstanding capability of the optimization algorithm once more in determining the boundaries, together with well-matched experimental and computational responses.

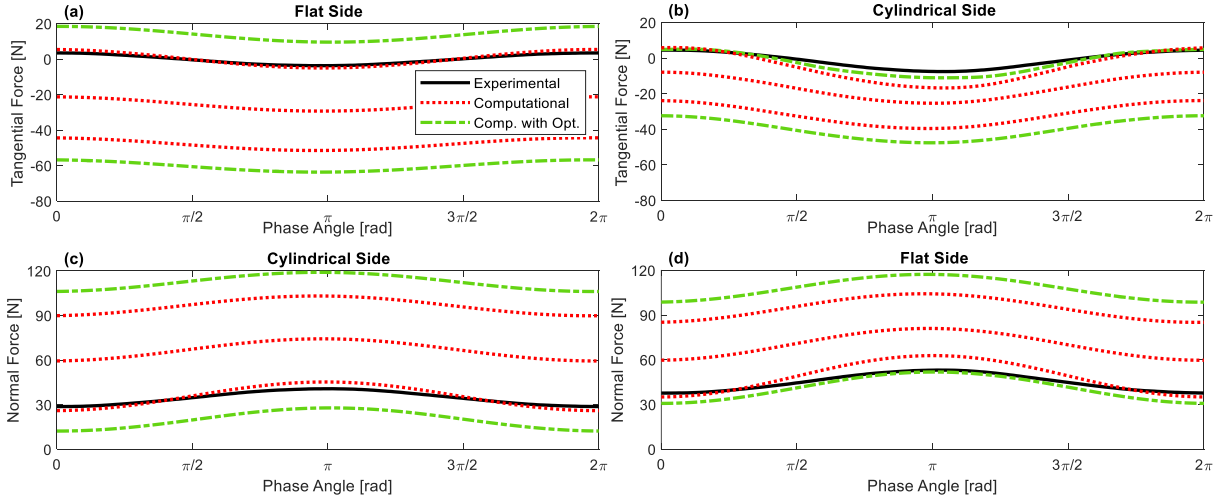

Fig. 17 Contact Forces on the Left Damper for 20 N Excitation Case at ω = 536 Hz

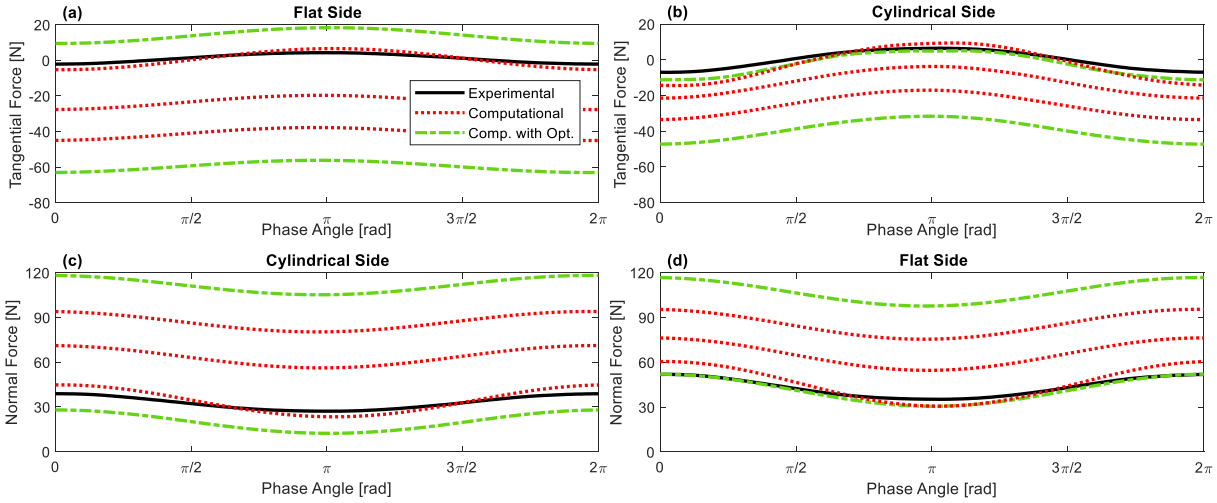

Fig. 18 Contact Forces on the Right Damper for 20 N Excitation Case at ω = 536 Hz

4.2.2 Multiple Nonlinear Responses with the Variability Range for 6.6 kg Pre-Load Cases

This case study includes the heaviest pre-load applied to the damper; hence the pressure on the contact surfaces is the largest among investigated ones. This provides the contact pairs in the model to better represent the actual scenario, since a node-to-node perfect match is theoretically assumed in the simulations.

Fig. 19 depicts all nonlinear responses measured and computed in the tests and simulations for different excitation amplitudes. A variability range is again clearly visible and it decreases with the increasing excitation level. The results show a great experimental-numerical match, as well as effective boundaries, also including the 100 N case. In addition to the general behavior of the frequency response, the resonance amplitudes are also given in Fig. 20 for a direct comparison; since most of the attention in the under-platform damper design is given to the maximum vibration levels as it is directly related to the maximum stress on the blade or the computation of the largest stresses. It is also interesting to note in Fig. 19 and Fig. 20 that the variability ranges for different excitation levels overlap, a phenomenon also observed for 4.6 kg case. This underlines the importance of the computation of multiple responses and boundaries. Otherwise, if the overall behavior is not captured and the attention is focused only to particular curves, one may incur in the misinterpretation of the system kinematics. It may even lead to observe a hardening behavior of the response with an increasing excitation level. For instance, the upper boundary of the 80 N case is higher than the lower boundary of the 50 N case, and these two responses can be obtained in two different particular analyses or

experiments. The correct inherent kinematics is only determined once the full range of variability has been tracked.

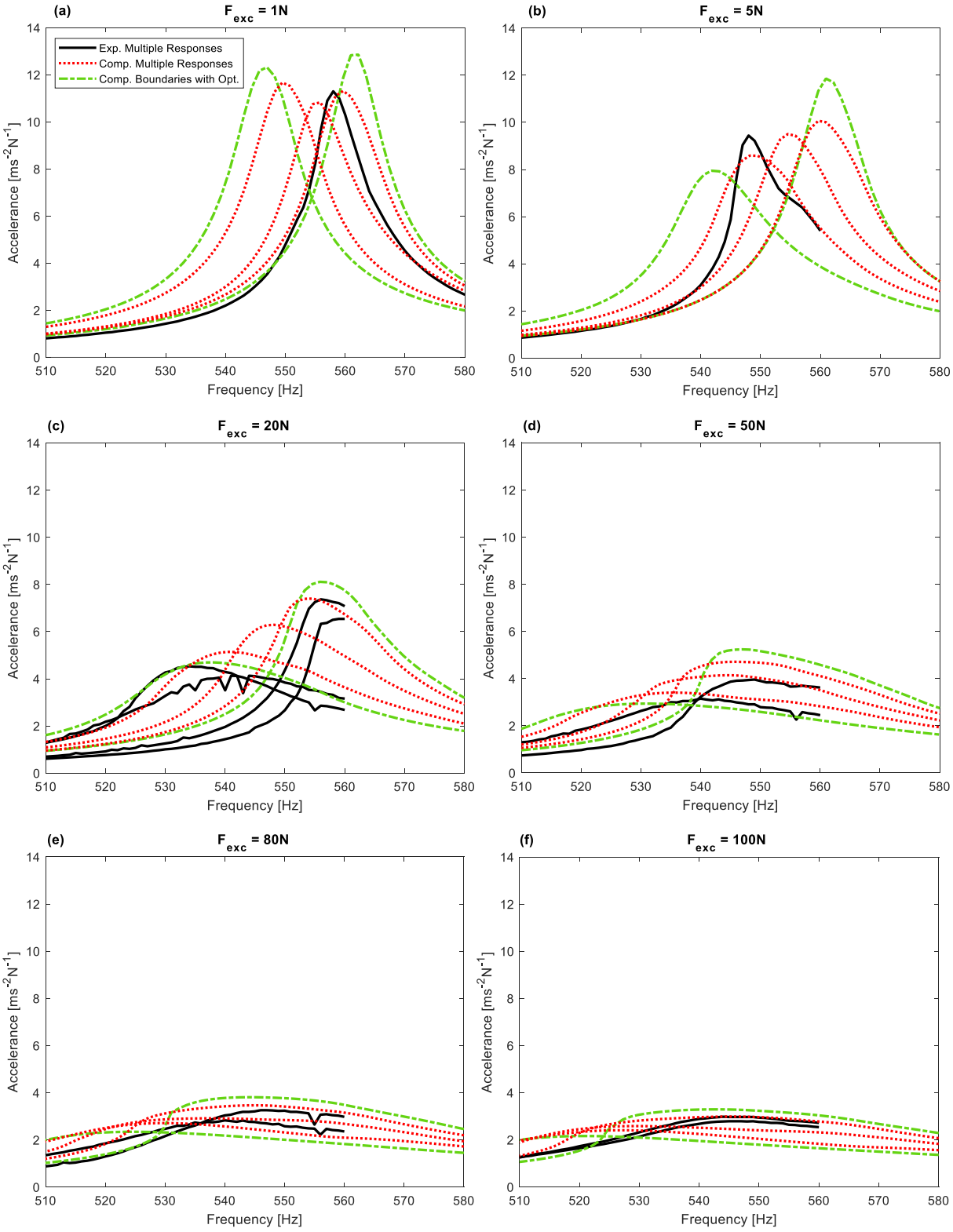

Fig. 19 Nonlinear Response Amplitude of the Blade Tip for Different Excitation Levels with 6.6 kg Pre-Load

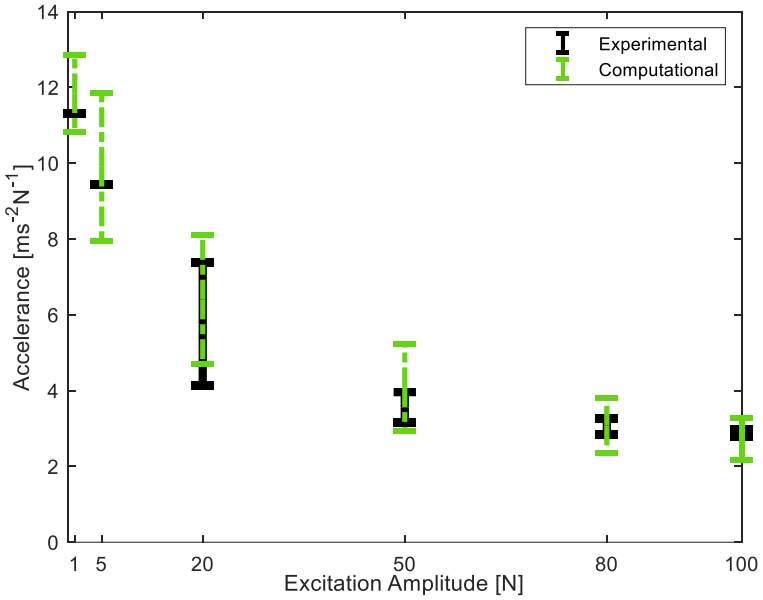

Fig. 20 The Variability Range of Resonance Response Amplitudes for Different Excitation Levels with 6.6 kg Pre-Load

Fig. 21 shows the evolution of loss factor which is used as the objective function to be minimized in the optimization algorithm. The solid line represents the values obtained during the computation of lower boundary, while dash-dotted line is for the upper boundary. As shown in Fig. 21, the value of the loss factor is bigger with larger excitation levels, since the number of slipping nodes increases as the forcing becomes large. This condition makes the dampers more dissipative, which results in higher proportions of dissipated energy over the stored energy, i.e. loss factor. It should also be noted that the lower boundary for a particular excitation level is characterized by bigger loss factors than those computed for the upper boundary. This is also relevant, because the contacts spend more time in the stick state during the analysis of upper boundary, while more slip occurs in the lower boundary case.

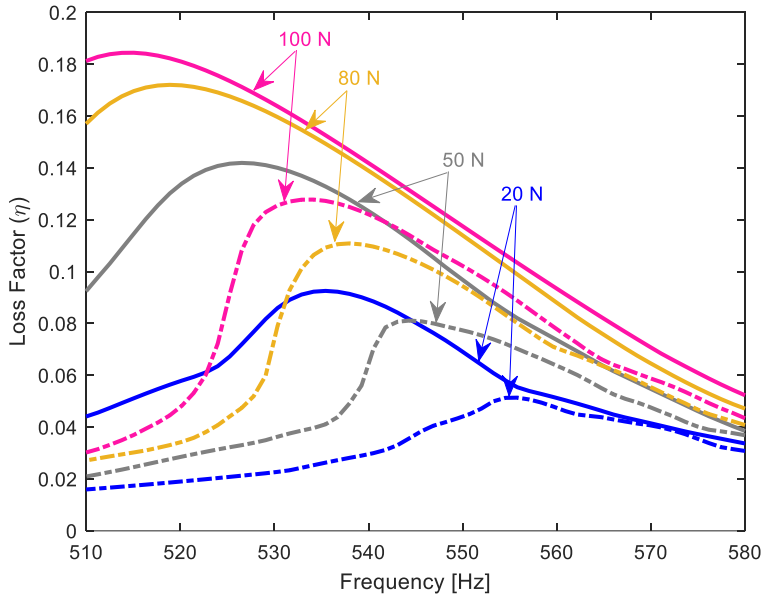

Fig. 21 Loss Factors corresponding to the Boundaries for Different Excitation Levels with 6.6 kg Pre-Load (Solid Line: Lower Boundary, Dash-dotted Line: Upper Boundary)

4.2.3 Multiple Nonlinear Responses with the Variability Range for 2.6 kg Pre-Load Cases

In this case, the pre-load is decreased to a smaller value (2.6 kg) to further challenge the numerical optimization method. Fig. 22 shows the nonlinear response amplitudes of the blade tip for various excitation levels. Although some of the experimental responses are captured computationally, the results are not as satisfactory as in the previous cases. The differences are clearer in the variability range of resonance response amplitudes, as shown in Fig. 23. It should be noted that this case with the lowest pre-load is the one where the nonlinearity is the largest. It is apparent that there is a missing point in the model, which provides a deviation between the experimental and computational results. Since the pre-load is very low, the contacts in the experiments may not be stable enough and some partial loss of contact may occur. Full contact may not have been achieved and the pressure distribution on the contact surfaces can be non-uniform. This explains the differences detected between the experimental response and the computational results, the latter being produced under the assumption of an ideal contact condition.

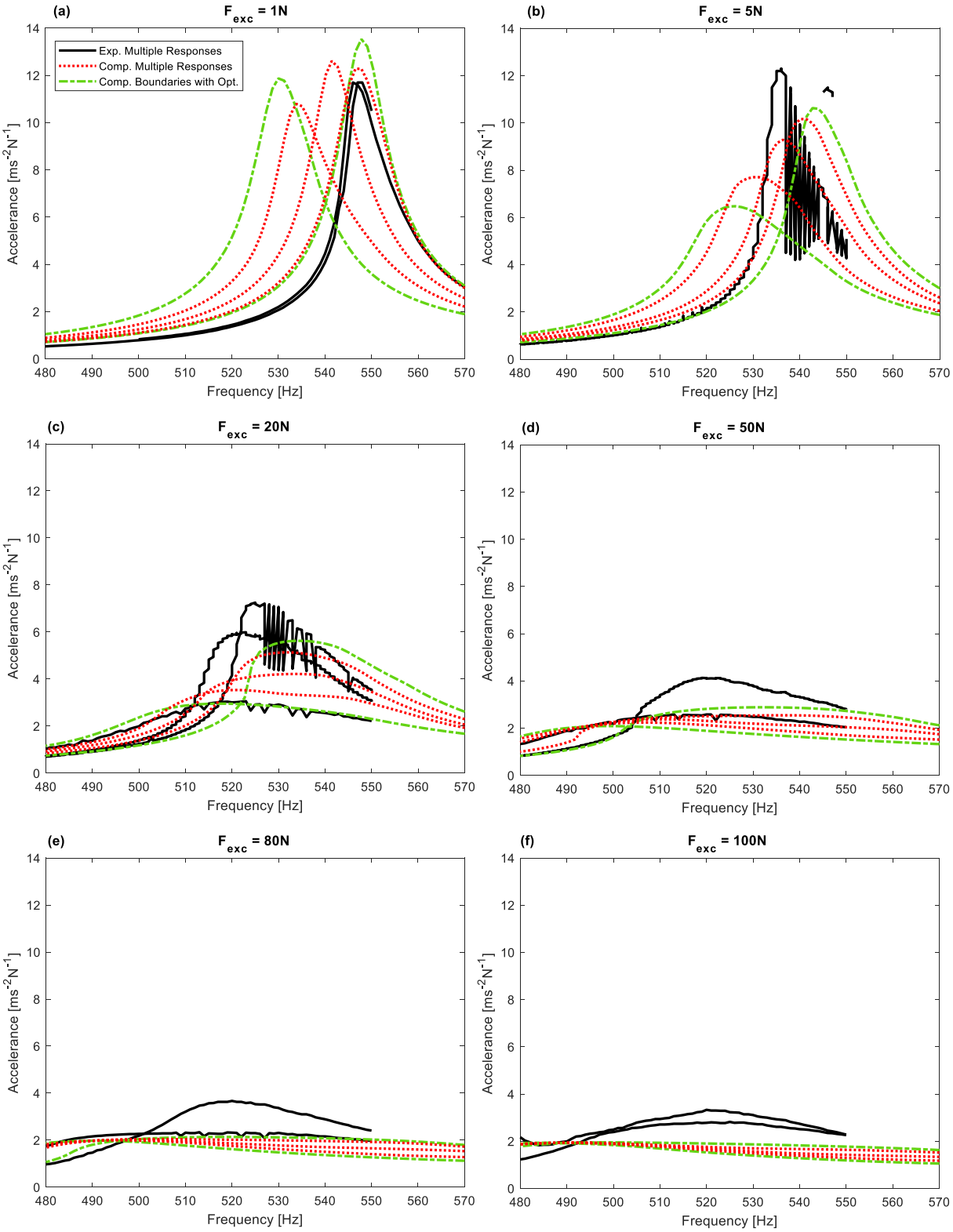

Fig. 22 Nonlinear Response Amplitude of the Blade Tip for Different Excitation Levels with 2.6 kg Pre-Load

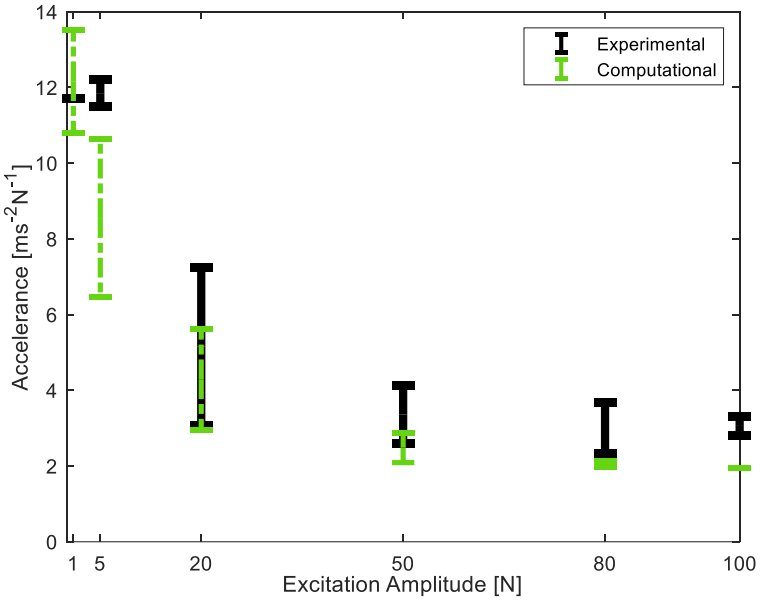

Fig. 23 The Variability Range of Resonance Response Amplitudes for Different Excitation Levels with 2.6 kg Pre-Load

5. CONCLUSION

A challenging issue in the structural dynamics community is to provide a satisfactory justification for the response variability in frictional systems. Most of the time, the main reason has been associated to several uncertainties; where one of them, the non-uniqueness of friction forces, is elaborately studied in this paper. In particular, a comparison between the experimental and computational results is performed, where the test data of variable responses and contact forces have already been measured in [16], while a numerical method developed very recently in [22] is utilized to estimate the boundaries of the variability range computationally. It is demonstrated in several cases that different static conditions with the same contact parameters and user-controlled inputs can give rise to a large variability in the nonlinear response, due to the non-uniqueness of friction forces. Experimental and computational results show a coherent parallelism for both frequency responses and variability ranges. This also supports the fact that the non-repeatability of the data is directly linked to the non-uniqueness uncertainty of contact forces. It is also demonstrated that the method proposed in [22] is fairly adequate to predict the experimentally measured variability range with the numerically calculated limits. Some deviations between the results, particularly for highly nonlinear cases, are also observed and presented. This indicates that the computational model should be tuned further with additional properties such as the inclusion of shaker-structure interaction, to fully mimic the non-ideal conditions achieved in the laboratory environment, which needs a sophisticated and a dedicated approach.

Non-uniqueness of contact forces is a phenomenon which has not received enough attention in the literature, although it has been firstly shown more than three decades ago. The current study underlines the importance of considering the non-unique contact forces, since fretting wear is not persuasive for the response variability of two consecutive tests. To the best of authors' knowledge, this study is the first one where a comparison is performed between experiments and simulations in the context of non-unique contact forces. This phenomenon needs more attention and requires further effort to better understand the contact kinematics. The engineers and researchers can become more aware of the effects of non-unique contact forces in the design of UPDs with the results of this study.

Acknowledgements

The authors would like to thank to Dr. Muhammad Umer for his previous contribution to the test rig design.

6. REFERENCES

[1] J.H. Griffin, Friction damping of resonant stresses in gas turbine engine airfoils, J. Eng. Power 102(2) (1980) 329-333. https://doi.org/10.1115/1.3230256.

[2] K.Y. Sanliturk, D.J. Ewins, A.B. Stanbridge, Underplatform dampers for turbine blades: theoretical modeling, analysis and comparison with experimental data, ASME J. Eng. Gas Turbines Power 123(4) (2001) 919-929. https://doi.org/10.1115/1.1385830.

[3] L. Panning , K. Popp , W. Sextro , F. Gotting , A. Kayser , I. Wolter, Asymmetrical underplatform dampers in gas turbine bladings: theory and application, Proceedings of the ASME Turbo Expo 2004: Power for Land, Sea, and Air. Volume 6: Turbo Expo 2004. Vienna, Austria. June 14–17, 2004. pp. 269-280. ASME. https://doi.org/10.1115/GT2004-53316

[4] E. Cigeroglu, N. An, C.H. Menq, Forced response prediction of constrained and unconstrained structures coupled through frictional contacts, ASME J. Eng. Gas Turbines Power 131(2) (2009): 022505. https://doi.org/10.1115/1.2940356.

[5] D. Laxalde, F. Thouverez, J.P. Lombard, Forced response analysis of ıntegrally bladed disks with friction ring dampers, J. Vib. Acoust. 132(1) (2010): 011013. https://doi.org/10.1115/1.4000763.

[6] R. Drozdowski, L. Völker, M. Häfele, D.M. Vogt, Experimental and numerical investigation of the nonlinear vibrational behavior of steam turbine last stage blades with friction bolt damping elements, In Turbo Expo: Power for Land, Sea, and Air, vol. 56796, p. V008T26A007. American Society of Mechanical Engineers, 2015. https://doi.org/10.1115/GT2015-42244.

[7] E. Denimal, C. Wong, L. Salles, L. Pesaresi, On the Efficiency of a Conical Underplatform Damper for Turbines, J. Eng. Gas Turbines Power. 143(2) (2021): 021020. https://doi.org/10.1115/1.4049665.

[8] I. A. Sever, E.P. Petrov, D. J. Ewins, Experimental and numerical investigation of rotating bladed disk forced response using underplatform friction dampers, J. Eng. Gas Turbines Power, 130(4) (2008): 042503. https://doi.org/10.1115/1.2903845.

[9] M. Claeys, J. J. Sinou, J. P. Lambelin, R. Todeschini, Modal interactions due to friction in the nonlinear vibration response of the "Harmony" test structure: Experiments and simulations, J Sound Vib. 376 (2016) 131-148. https://doi.org/10.1016/j.jsv.2016.04.008

[10] M. R. W. Brake, C. W. Schwingshackl, P. Reuß, Observations of variability and repeatability in jointed structures, Mech. Syst. Signal Process. 129 (2019) 282-307. https://doi.org/10.1016/j.ymssp.2019.04.020.

[11] V. Janovský, Catastrophic features of Coulomb friction model. The mathematics of Finite Elements and Applications (1981) 259-264.

[12] E. N. Mitsopoulou, I. N. Doudoumis, A contribution to the analysis of unilateral contact problems with friction. Solid Mechanics Archives, 12(3) (1987) 165-186.

[13] A. Klarbring, Examples of non-uniqueness and non-existence of solutions to quasistatic contact problems with friction. Ingenieur-Archiv, 60(8) (1990) 529-541.

[14] B.D. Yang, C.H. Menq, Characterization of contact kinematics and application to the design of wedge dampers in turbomachinery blading: part 1—stick-slip contact kinematics, J. Eng. Gas Turbines Power 120(2) (1998) 410-417. https://doi.org/10.1115/1.2818138.

[15] D. Botto, M. Umer, A novel test rig to investigate under-platform damper dynamics, Mech. Syst. Signal Process. 100 (2018) 344-359. https://doi.org/10.1016/j.ymssp.2017.07.046.

[16] D. Botto, C. Gastaldi, M.M. Gola, M. Umer, An experimental ınvestigation of the dynamics of a blade with two under-platform dampers, J. Eng. Gas Turbines Power 140(3) (2018): 032504. https://doi.org/10.1115/1.4037865.

[17] B.D. Yang, C.H. Menq, Characterization of contact kinematics and application to the design of wedge dampers in turbomachinery blading: part 2—prediction of forced response and experimental verification, J. Eng. Gas Turbines Power 120(2) (1998) 418-423. https://doi.org/10.1115/1.2818139.

[18] S. Zucca, D. Botto, M.M. Gola, Range of variability in the dynamics of semi-cylindrical friction dampers for turbine blades, Proceedings of the ASME Turbo Expo 2008: Power for Land, Sea, and Air. Volume 5: Structures and Dynamics, Parts A and B. Berlin, Germany. June 9–13, 2008. pp. 519-529. https://doi.org/10.1115/GT2008-51058.

[19] C. Gastaldi, J. Gross, M. Scheel, T. M. Berruti, M. Krack, Modeling complex contact conditions and their effect on blade dynamics, J. Eng. Gas Turbines Power 143(1): 011007. https://doi.org/10.1115/1.4049186.

[20] E. Ferhatoglu, S. Zucca, D. Botto, J. Auciello, L. Arcangeli, Nonlinear vibration analysis of turbine bladed disks with mid-span dampers, J. Eng. Gas Turbines Power GTP-21-1567. https://doi.org/10.1115/1.4053107.

[21] E. Ferhatoglu, S. Zucca, Determination of periodic response limits among multiple solutions for mechanical systems with wedge dampers, J Sound Vib. 494 (2021) 115900. https://doi.org/10.1016/j.jsv.2020.115900.

[22] E. Ferhatoglu, S. Zucca, On the non-uniqueness of friction forces and the systematic computation of dynamic response boundaries for turbine bladed disks with contacts, Mech. Syst. Signal Process. 160 (2021): 107917. https://doi.org/10.1016/j.ymssp.2021.107917.

[23] W. Sextro, K. Popp, I. Wolter, Improved reliability of bladed disks due to friction dampers, Proceedings of the ASME 1997 International Gas Turbine and Aeroengine Congress and Exhibition. Volume 4: Manufacturing Materials and Metallurgy; Ceramics; Structures and Dynamics; Controls, Diagnostics and Instrumentation; Education; IGTI Scholar Award. Orlando, Florida, USA. June 2–5, 1997. https://doi.org/10.1115/97-GT-189.

[24] L. Pesaresi, L. Salles, A. Jones, J.S. Green, C.W. Schwingshackl, Modelling the nonlinear behaviour of an underplatform damper test rig for turbine applications, Mech. Syst. Signal Process. 85 (2017) 662-679. https://doi.org/10.1016/j.ymssp.2016.09.007.

[25] R.R. Craig JR, M.C.C. Bampton, Coupling of substructures for dynamic analyses, AIAA J. 6(7) (1968) 1313-1319. https://doi.org/10.2514/3.4741.

[26] G.M. Jenkins, Analysis of the stress–strain relationships in reactor grade graphite. Br. J. Appl. Phys. 13(1) (1962) 30. https://doi.org/10.1088/0508-3443/13/1/307.

[27] C. Gastaldi, M. M. Gola, An improved microslip model for variable normal loads, In: Pennacchi P. (eds) Proceedings of the 9th IFToMM International Conference on Rotor Dynamics. Mechanisms and Machine Science, 21 (2015) 169-179. https://doi.org/10.1007/978-3-319-06590-8_14.

[28] C. Gastaldi, M. M. Gola, On the relevance of a microslip contact model for under-platform dampers, Int. J. Mech. Sciences 115-116 (2016) 145-156. https://doi.org/10.1016/j.ijmecsci.2016.06.015.

[29] E. Ciğeroğlu, H. N. Özgüven, Nonlinear vibration analysis of bladed disks with dry friction dampers, J Sound Vib. 295 (2006) 1028-1043. https://doi.org/10.1016/j.jsv.2006.02.009.

[30] N. Jamia, H. Jalali, J. Taghipour, M.I. Friswell, H. Haddad Khodaparast, An equivalent model of a nonlinear bolted flange joint, Mech. Syst. Signal Process. 153 (2021) 107507. https://doi.org/10.1016/j.ymssp.2020.107507.

[31] C. Gastaldi, M. M. Gola, Testing, simulating and understanding under-platform damper dynamics, In Proceedings of the VII European Congress on Computational Methods in Applied Sciences and Engineering, Crete, Greece (2016) 5-10. https://doi.org/10.7712/100016.2134.11184.

[32] C. Gastaldi, Modeling friction for turbomachinery applications: tuning techniques and adequacy assessment of heuristic contact models. Contact and Fracture Mechanics, 97. (2018).

[33] C. Siewert, L. Panning, J. Wallaschek, C. Richter, Multiharmonic forced response analysis of a turbine blading coupled by nonlinear contact forces, J. Eng. Gas Turbines Power 132(8) (2010): 082501. https://doi.org/10.1115/1.4000266.

[34] T.M. Cameron, J.H. Griffin, An alternating frequency/time domain method for calculating the steady-state response of nonlinear dynamic systems, J. Appl. Mech. 56(1) (1989) 149-154. https://doi.org/10.1115/1.3176036.

[35] C. Siewert, L. Panning, C. Gerber, P.A. Masserey, Numerical and experimental damping prediction of a nonlinearly coupled low pressure steam turbine blading, Proceedings of the ASME Turbo Expo 2008: Power for Land, Sea, and Air. Volume 5: Structures and Dynamics, Parts A and B. Berlin, Germany. June 9–13, 2008. pp. 531-542. https://doi.org/10.1115/GT2008-51073.

[36] J. Chen, C. Zang, B. Zhou, E.P. Petrov, High-fidelity calculation of modal damping caused by friction at blade roots for single blades and tuned bladed disc assemblies, Proceedings of the Institution of Mechanical Engineers, Part C: Journal of Mechanical Engineering Science, June 2020. https://doi.org/10.1177/0954406220935144.

[37] E.P. Petrov, A method for use of cyclic symmetry properties in analysis of nonlinear multiharmonic vibrations of bladed disks, J. Turbomach. 126 (1) (2004) 175–183, https://doi.org/10.1115/1.1644558.

[38] R.H. Byrd, M.E. Hribar, J. Nocedal, An interior point algorithm for large-scale nonlinear programming, SIAM Journal on Optimization 9(4) (1999) 877-900. https://doi.org/10.1137/S1052623497325107.

[39] R.H. Byrd, J.C. Gilbert, J. Nocedal, A trust region method based on interior point techniques for nonlinear programming, Math. Program. 89 (2000) 149-185. https://doi.org/10.1007/PL00011391.

[40] S. Medina, D. Nowell, D. Dini, Analytical and numerical models for tangential stiffness of rough elastic contacts, Tribology Letters 49(1) (2013) 103-115. https://doi.org/10.1007/s11249-012-0049-y.

[41] K. S. Parel, R. J. Paynter, D. Nowell, Linear relationship of normal and tangential contact stiffness with load. Proceedings of the Royal Society A, 476(2243) (2020) 20200329. https://doi.org/10.1098/rspa.2020.0329.